NRC·CNRC

NRC Publications Archive
Archives des publications du CNRC

Models of optical characteristics of barrel-vault skylights: development, validation and application

Laouadi, A.

This publication could be one of several versions: author's original, accepted manuscript or the publisher's version. / La version de cette publication peut être l'une des suivantes : la version prépublication de l'auteur, la version acceptée du manuscrit ou la version de l'éditeur.
For the publisher's version, please access the DOI link below./ Pour consulter la version de l'éditeur, utilisez le lien DOI ci-dessous.

Publisher's version / Version de l'éditeur:
https://doi.org/10.1191/1365782805li141oa
Lighting Research & Technology, 37, September 3, pp. 235-264, 2005-09-01

NRC Publications Record / Notice d'Archives des publications de CNRC:
https://nrc-publications.canada.ca/eng/view/object/?id=cc784fc4-8ad1-4370-bff0-ce0f458d5411
https://publications-cnrc.canada.ca/fra/voir/objet/?id=cc784fc4-8ad1-4370-bff0-ce0f458d5411

Access and use of this website and the material on it are subject to the Terms and Conditions set forth at https://nrc-publications.canada.ca/eng/copyright
READ THESE TERMS AND CONDITIONS CAREFULLY BEFORE USING THIS WEBSITE.

L'accès à ce site Web et l'utilisation de son contenu sont assujettis aux conditions présentées dans le site https://publications-cnrc.canada.ca/fra/droits
LISEZ CES CONDITIONS ATTENTIVEMENT AVANT D'UTILISER CE SITE WEB.

Questions? Contact the NRC Publications Archive team at PublicationsArchive-ArchivesPublications@nrc-cnrc.gc.ca. If you wish to email the authors directly, please see the first page of the publication for their contact information.

Vous avez des questions? Nous pouvons vous aider. Pour communiquer directement avec un auteur, consultez la première page de la revue dans laquelle son article a été publié afin de trouver ses coordonnées. Si vous n'arrivez pas à les repérer, communiquez avec nous à PublicationsArchive-ArchivesPublications@nrc-cnrc.gc.ca.

National Research Council Canada | Conseil national de recherches Canada

Canada

National Research Council Canada | Conseil national de recherches Canada

NRC · CNRC

Models of optical characteristics of barrel-vault skylights: development, validation and application

Laouadi, A.

NRCC-47289

A version of this document is published in / Une version de ce document se trouve dans :
Lighting Research & Technology, v. 37, no. 3, Sept. 2005, pp. 235-264
Doi: 10.1191/1365782805li141oa

http://irc.nrc-cnrc.gc.ca/ircpubs

construction Institute for Research in Construction | Institut de recherche en construction IRC

MODELS OF OPTICAL CHARACTERISTICS OF BARREL VAULT SKYLIGHTS: DEVELOPMENT, VALIDATION AND APPLICATION

Abdelaziz Laouadi

Indoor Environment Research Program

Institute for Research in Construction

National Research Council Canada

1200 Montreal Road, Ottawa, Ontario, Canada, K1A 0R6

Fax: +1 613 954 3733

Tel: +1 613 990 6868

Email: aziz.laouadi@nrc-cnrc.gc.ca

ABSTRACT

By admitting natural light deep into a building and connecting occupants with the outside, skylights can improve the aesthetic look of buildings and increase occupant satisfaction. In addition, by allowing the entry of natural light electric light levels can be reduced thereby leading to energy savings. However, the potential energy benefits and amenities of skylights have not been fully exploited in today's building design due to some theoretical and technical challenges. The lack of design tools is one of the major hurdles building designers face to adopt such products and quantify their energy benefits. The optical characteristics of skylights are the significant factors affecting their energy benefits. Recognizing this gap, the SkyVision tool was developed to assist skylight manufacturers and building designers in developing appropriate skylight designs for given building types and daylighting applications. This paper describes the models implemented in SkyVision to compute the optical characteristics of barrel vault skylights with clear, fully translucent or partially diffusing glazing under beam and diffuse light. The models are based on the ray-tracing technique. Under diffuse light, two models are developed: (1) a luminance-based model when the sky luminance distribution is known, and (2) an illuminance-based model when the illuminance on a horizontal surface is rather known. The second model is simpler and faster and more suitable for annual performance calculation. Experimental measurements of the skylight transmittance were conducted under real sky conditions to validate the model predictions. The actual measurements compared reasonably well with the model predictions. The predictions from the luminance-based and illuminance-based models showed good agreement with each other. When applied to an example study, the models predicted that vault skylights with clear glazing are more effective than flat skylights with similar glazing in boosting the beam light transmittance, particularly in winter days. Translucent vault skylights are more effective than flat skylights with similar glazing in reducing solar heat gains, particularly in summer days. Translucent skylights may out-perform transparent skylights, particularly during sunny days in winter.

List of Symbols

A_1, A_2 : designate the geometry of the side surfaces of the skylight

A_3 : designates the geometry of the top surface of the skylight

A_{11} : portion of surface A_1 through which solar rays undergo only direct transmission

A_{12} : portion of surface A_1 through which solar rays undergo transmission and inter-reflection

A_{31} : portion of surface A_3 through which solar rays undergo only direct transmission

A_{32} : portion of surface A_3 through which solar rays undergo transmission and inter-reflection

E : illuminance (lux)

F_{kj} : view factor of surface k to surface j (dimensionless)

F_{kb} : view factor of surface k to the skylight base surface (dimensionless)

F_{sb} : view factor of skylight surface to its base surface (dimensionless)

F_1, F_2 : coefficients for the circumsolar and horizon brightening components of the Perez et al. model[17], respectively (dimensionless)

G : reflection function, equation (31), (dimensionless)

L : skylight length (m)

N : total number of reflections from the side surfaces of skylight

$\bar{N}$: average of N over a given surface

n : number of reflections from a given surface

$\bar{n}$: average of n over a given surface

Q_0 : initial flux exiting a surface (lumens)

QT_{vault} : transmitted flux through the skylight (lumens)

QA_{vault} : absorbed flux by the skylight (lumens)

QT_d : diffuse component of the transmitted flux through the skylight for an arbitrary sun position (lumens)

QA_d : diffuse component of the absorbed flux by the skylight for an arbitrary sun position (lumens)

QT_{par} : transmitted flux when the sun's rays are parallel to the skylight axis (lumens)

$QT_{b,par}$: beam component of QT_{par} (lumens)

$QT_{d,par}$: diffuse component of QT_{par} (lumens)

QA_{par} : absorbed flux when the sun's rays are parallel to the skylight axis (lumens)

$QA_{b,par}$: beam component of QA_{par} (lumens)

$QA_{d,par}$: diffuse component of QA_{par} (lumens)

QT_{per} : transmitted flux when the sun's rays are perpendicular to the skylight axis (lumens)

$QT_{b,per}$: beam component of QT_{per} (lumens)

$QT_{d,per}$: diffuse component of QT_{per} (lumens)

QA_{per} : absorbed flux when the sun's rays are perpendicular to the skylight axis (lumens)

$QA_{b,per}$: beam component of QA_{per} (lumens)

$QA_{d,per}$: diffuse component of QA_{per} (lumens)

R : skylight radius (m)

S : surface area (m^2)

W : weighting function, equation (70), (dimensionless)

y : y-position of a point moving on the skylight surface

Greek Symbols

Γ : sky point luminance (cd/m^2)

α : surface absorptance (dimensionless)

β : surface inclination angle from the horizontal (radians)

ε : ratio of the incident flux on a skylight surface to that incident on a horizontal flat surface (dimensionless)

γ : portion of the surface transmitted flux that directly reaches the base surface of the skylight, expressed relative to a perfectly diffusing surface (dimensionless)

$\bar{\gamma}$: average value of γ over a given skylight surface

θ : incidence angle on a surface (radians)

θ_z : sun zenith angle (radians)

θ_h : sun altitude angle, $\theta_h = \pi/2 - \theta_z$, (radians)

ρ : surface reflectance (dimensionless)

σ : position angle of a point on the skylight surface (radians)

σ_0 : skylight truncation angle (radians)

τ : surface transmittance (dimensionless)

ψ_0 : skylight's axis azimuth angle with respect to the south direction (radians)

ψ_s : solar azimuth angle with respect to the south direction (radians)

Subscripts

b : beam component, or back of surface

bb : beam beam component

bd : beam diffuse component

d : diffuse light

eq : optically equivalent to a flat skylight

f : front of surface

gr : ground

i : incident

k : surface index

par : sun's rays parallel to the skylight axis

per : sun's rays perpendicular to the skylight axis

r : inter-reflected

t : transmitted

1 Introduction

Barrel vault skylights are typically found in commercial and institutional buildings such as shopping malls, atriums, schools, swimming pools, etc. They connect building occupants to the outside and provide the indoor space with natural illumination and solar heat gains. Properly designed skylights may save a substantial amount of energy for lighting, heating and cooling[1,2]. Recent research has shown that the skylight shape and glazing type can significantly alter the skylight energy performance[1-3]. The air space directly underneath the skylight may reduce the solar heat gains by up to 25%[4], and the annual cooling energy by up to 6%[5]. Furthermore, some studies around the world showed that skylights may improve non-energy aspects of buildings such as retail sales[6, 7].

However, the potential energy benefits and amenities of skylights have not been fully exploited in today's building designs due to some theoretical and technical challenges. The lack of design tools is one of the major hurdles building designers face to adopt such products and quantify their energy benefits. Currently available fenestration simulation software such as FRAMEplus5.1[8] and WINDOW5.1[9] deal with only planar and transparent geometry, such as windows and flat skylights. Sophisticated lighting simulation software such as RADIANCE[10], LUMEN MICRO[11] and SUPERLITE[12] are not only cumbersome to use, but they do not provide any output related to the skylight optical characteristics required for product rating and selection. Specialized skylight software are very rare and limited. The SkyCalc program[13] is limited to some USA climate regions, and handles only flat translucent skylights.

Recognizing the limitations of the current fenestration computer tools, we developed SkyVision, a specialized computer program to predict skylight performance. The SkyVision tool aims at assisting skylight manufacturers and building designers to come up with an appropriate skylight design for a given building type and use. The tool analyses the optical characteristics of skylights of various shapes and types, and calculates their daylighting and energy performance. To maximize the energy benefits of skylights, SkyVision accounts for the lighting and shading controls, skylight shape, size and glazing type, curb/well geometry, building location and orientation, and prevailing climate. It is intended for use by skylight manufacturers, building designers, architects, engineers, fenestration councils, and research and educational institutions. SkyVision is available free of charge from the web site: *http://irc.nrc-cnrc.gc.ca/ie/light/skyvision.*

The aim of this paper is to describe the development, validation, and application of the models implemented in SkyVision to predict the optical characteristics (transmittance, absorptance and reflectance) of barrel vault skylights.

2 Objectives

The specific objectives of this paper are:

- To develop analytical models to predict the optical characteristics of barrel vault skylights with clear, fully translucent, or partially-diffusing glazing under beam and diffuse light (section 3);
- To conduct experiments to measure the visible transmittance of a barrel vault skylight (section 4);
- To compare the measurements with the model predictions (section 5.1);
- To apply the models to predict the visible transmittance of a barrel vault skylight under typical summer and winter days (section 5.2); and
- To compare the performance of the developed luminance-based and illuminance-based models (section 5.3).

3 Mathematical Formulation

A barrel vault skylight is made of three glazed surfaces: a top cylindrical surface (A_3), and two side surfaces (A_1 and A_2). The skylight is geometrically defined by the truncation angle (σ_0), radius (R) and length (L). The axis of the cylindrical surface may be oriented with an azimuth angle ψ_0 with respect to the south direction. Each skylight surface may take on a different glazing type. The surface glazing may be multi-pane partially diffusing or clear. Partially diffusing glazing is commonly found in skylights, particularly skylights with plastic glazing. Figure 1 shows a schematic description of a barrel vault skylight.

Analytical models based on the ray-tracing technique have been developed to predict the overall optical characteristics of transparent barrel vault skylights under beam light[3]. The same ray-tracing technique was also applied to other skylight shapes[14, 15]. In the following, the previously developed models are extended to cover the optical characteristics of skylights with partially diffusing glazing under beam and diffuse light.

3.1 Beam Light Transmission

Tracing a given ray as it transmits through and reflects from the skylight surfaces is very complex to handle analytically. To simplify the problem, an approach is used to find mathematically well-defined surfaces so that the result of the ray tracing can be easily handled in a closed form formulation. In this regard, two positions of the sun's rays with respect to the skylight are identified: sun's rays parallel and

perpendicular to the skylight axis (y). When the sun's rays are in between the two positions, an interpolation formula is used.

3.1.1 Sun's Rays Parallel to the Skylight Axis

Figure 2 shows a schematic description of the beam light transmission through a clear skylight when the sun's rays are parallel to the skylight axis (y). In tracing the beam light transmission, the individual skylight surfaces are split into two portions. One portion corresponds to the directly-transmitted component where the incident rays undergo only transmission to reach the skylight base surface. The second portion corresponds to the transmitted-reflected component where the incident rays undergo transmission and inter-reflections from the skylight interior surfaces to reach the skylight base surface. Since the skylight glazing is partially diffusing, the glazing transmission or reflection for the beam light is made up of two components: beam and diffuse. Any transmitted or inter-reflected flux will therefore be made up of two components: beam and diffuse. The beam component follows the direction of the incident rays whereas the diffuse component is assumed to be uniformly spread in all directions.

The following analysis assumes that the sun position is within the quadrants of the side surface A_1, that is only surfaces A_1 and A_3 are exposed to the sun's rays. This happens when the skylight azimuth angle with respect to the solar azimuth satisfies: $0 \le |\psi_s-\psi_0| \le \pi/2$, or $3\pi/2 < |\psi_s-\psi_0| \le 2\pi$. When the sun position is within the quadrants of the side surface A_2, (i.e., $\pi/2 < |\psi_s-\psi_0| \le 3\pi/2$), the analysis also holds by exchanging the surface index 1 with 2 and vice versa.

The incident beam flux on a horizontal skylight is given by the following equation:

$$Q_{par} = \int_{A_1} E_b \cos\theta \cdot ds + \int_{A_3} E_b \cos\theta \cdot ds \tag{1}$$

where E_b is the normal beam illuminance, ds is an elementary surface, and θ is the incidence angle on the elementary surface.

The incidence angle (θ) on an inclined surface is given by the following equation[16]:

$$\cos\theta = \cos\theta_z \cdot \cos\beta + \sin\theta_z \cdot \sin\beta \cdot \cos(\psi_s - \psi) \tag{2}$$

where β is the inclination angle of the surface from the horizontal (varies from 0 to $\pi/2$ radians), ψ is the surface azimuth angle with respect to the south direction, positive west of south and negative east of south (varies from $-\pi$ to π radians), and ψ_s is the solar azimuth angle.

The skylight surfaces A_1 (or A_2) and A_3 are defined as follows:

$$A_1 : \{\sigma_0 \le \sigma \le \pi - \sigma_0; \quad \beta = \pi/2; \quad \psi - \psi_s = 0\} \tag{3}$$

$$A_3 : \{0 \le y \le L; \quad \sigma_0 \le \sigma \le \pi - \sigma_0; \quad \beta = |\pi/2 - \sigma|; \quad \psi - \psi_s = \pm\pi/2\} \tag{4}$$

where σ is the position angle of a point on the skylight surface A_3, and σ_0 is the skylight truncation angle (varies from 0 to $\pi/2$ radians).

For a collimated beam light such as sunlight, the normal beam illuminance (E_b) does not vary with the surface inclination and azimuth angles. Thus, equation (1) reduces to:

$$Q_{par} = E_b \cdot S_1 \sin\theta_z + E_b \cdot S_h \cos\theta_z \tag{5}$$

where S_1 is the area of surface A_1, and S_h is the area of the skylight base surface (aperture surface).

Since the skylight glazing is partially diffusing, the transmitted and absorbed beam flux is made up of two components – beam and diffuse, given by the following equations:

$$QT_{par} = QT_{b,par} + QT_{d,par} \tag{6}$$

$$QA_{par} = QA_{b,par} + QA_{d,par} \tag{7}$$

where $QT_{b,par}$ and $QT_{d,par}$ are the beam and diffuse components of the transmitted flux (QT_{par}) for the parallel configuration, respectively; and $QA_{b,par}$ and $QA_{d,par}$ are the beam and diffuse components of the absorbed flux (QA_{par}) for the parallel configuration, respectively.

By following the ray tracing technique, one obtains the beam and diffuse components of the transmitted and absorbed flux as follows:

$$\begin{aligned} QT_{b,par}/E_b = &\int_{A_{11}} \tau_{bb,1}(\theta)\cdot\cos\theta\cdot ds + \int_{A_{12}} \tau_{bb,1}(\theta)\cdot\rho_{bb,2,b}^{n_2}(\theta)\cdot\rho_{bb,1,b}^{n_1}(\theta)\cos\theta\cdot ds \\ &+ \int_{A_{31}} \tau_{bb,3}(\theta)\cdot\cos\theta\cdot ds + \int_{A_{32}} \tau_{bb,3}(\theta)\cdot\rho_{bb,2,b}^{n_2}(\theta_h)\cdot\rho_{bb,1,b}^{n_1}(\theta_h)\cos\theta\cdot ds \end{aligned} \tag{8}$$

$$QT_{d,par} = \sum_{k=1}^{3} Q_{d,k} F_{kb} \tag{9}$$

$$\begin{aligned} QA_{b,par}/E_b = &\int_{A_1} \alpha_{1,f}(\theta)\cdot\cos\theta\cdot ds + \int_{A_{12}} \tau_{bb,1}(\theta)\cdot\left[\alpha_{2,b}(\theta)\cdot G(n_2) + \alpha_{1,b}(\theta)\cdot\rho_{bb,2,b}(\theta)\cdot G(n_1)\right]\cdot\cos\theta\cdot ds \\ &+ \int_{A_3} \alpha_{3,f}(\theta)\cdot\cos\theta\cdot ds + \int_{A_{32}} \tau_{bb,3}(\theta)\cdot\left[\alpha_{2,b}(\theta_h)\cdot G(n_2) + \alpha_{1,b}(\theta_h)\cdot\rho_{bb,2,b}(\theta_h)\cdot G(n_1)\right]\cdot\cos\theta\cdot ds \end{aligned} \tag{10}$$

$$QA_{d,par} = \sum_{k=1}^{3} \left(Q_{d,k} - Q_{0,k}\right)\cdot\alpha_{d,k,b}/\rho_{d,k,b} \tag{11}$$

where A_{11}, A_{12} are the portions of surface A_1 that correspond to the directly-transmitted and transmitted-reflected light flux, respectively; A_{31}, A_{32} are the portions of surface A_3 that correspond to the directly-transmitted and transmitted-reflected flux, respectively; F_{kb} is the view factor of surface A_k to the skylight base surface, G is a reflection function, given by equation (31); $Q_{d,k}$ is the diffuse flux exiting from surface A_k; n_k is the number of reflections from surfaces A_k; $\alpha_{k,f}$ and $\alpha_{k,b}$ are the front and back absorptances of surface A_k; $\rho_{bb,k,b}$ and $\rho_{bd,k,b}$ are the beam and diffuse components of the back reflectance of surface A_k ($\rho_{k,b} = \rho_{bb,k,b} + \rho_{bd,k,b}$); $\tau_{bb,k}$ and $\tau_{bd,k}$ are the beam and diffuse components of the transmittance of surface A_k ($\tau_k = \tau_{bb,k} + \tau_{bd,k}$); and θ_h is the sun altitude angle ($\theta_h = \pi/2 - \theta_z$).

By using the net radiation method, one obtains the following equations for the diffuse flux:

$$Q_{d,1} - \rho_{d,1,b}F_{21}Q_{d,2} - \rho_{d,1,b}F_{31}Q_{d,3} = Q_{0,1} \tag{12}$$

$$-\rho_{d,2,b}F_{12}Q_{d,1} + Q_{d,2} - \rho_{d,2,b}F_{32}Q_{d,3} = Q_{0,2} \tag{13}$$

$$-\rho_{d,3,b}F_{13}Q_{d,1} - \rho_{d,3,b}F_{23}Q_{d,2} + \left(1 - \rho_{d,3}F_{33}\right)Q_{d,3} = Q_{0,3} \tag{14}$$

where F_{kj} designates the view factor from surface A_k to surface A_j, and $Q_{0,k}$ is the initial flux (before the diffuse inter-reflection) exiting the surface A_k. The initial flux is made up of the diffuse transmitted and inter-reflected flux, expressed in the following equations:

$$Q_{0,k} = Q_{0,k,t,par} + Q_{0,k,r,par}; \quad k = 1 \text{ to } 3 \tag{15}$$

where $Q_{0,k,t,par}$ and $Q_{0,k,r,par}$ stand for the diffuse transmitted and inter-reflected initial flux of surface A_k for the parallel configuration, respectively.

Following the ray tracing technique, the diffuse transmitted and inter-reflected initial flux is given by the following equations:

$$Q_{0,1,t,par} = \int_{A_1} E_b \cdot \tau_{bd,1}(\theta) \cdot \cos\theta \cdot ds \tag{16}$$

$$\begin{aligned} Q_{0,1,r,par} = & \int_{A_{12}} E_b \cdot \tau_{bb,1}(\theta) \cdot \rho_{bb,2,b}(\theta) \cdot \rho_{bd,1,b}(\theta) \cdot G(n_1) \cdot \cos\theta \cdot ds \\ & + \int_{A_{32}} E_b \cdot \tau_{bb,3}(\theta) \cdot \rho_{bb,2,b}(\theta_h) \cdot \rho_{bd,1,b}(\theta_h) \cdot G(n_1) \cdot \cos\theta \cdot ds \end{aligned} \tag{17}$$

$$Q_{0,2,t,par} = 0 \tag{18}$$

$$Q_{0,2,r,par} = \int_{A_{12}} E_b \cdot \tau_{bb,1}(\theta) \cdot \rho_{bd,2,b}(\theta) \cdot G(n_2) \cdot \cos\theta \cdot ds + \int_{A_{32}} E_b \cdot \tau_{bb,3}(\theta) \cdot \rho_{bd,2,b}(\theta_h) \cdot G(n_2) \cdot \cos\theta \cdot ds \tag{19}$$

$$Q_{0,3,t,par} = \int_{A_3} E_b \cdot \tau_{bd,3}(\theta) \cdot \cos\theta \cdot ds; \qquad Q_{0,3,r,par} = 0 \tag{20}$$

The surface portions A_{11} , A_{12}, A_{31} and A_{32} are defined as follows:

$$A_{11} : \{\sigma_0 \le \sigma \le \sigma_1; \quad \pi - \sigma_1 \le \sigma \le \pi - \sigma_0; \quad \beta = \pi/2; \quad \psi - \psi_s = 0\} \tag{21}$$

$$A_{12} : \{\sigma_1 < \sigma < \pi - \sigma_1; \quad \beta = \pi/2; \quad \psi - \psi_s = 0\} \tag{22}$$

$$A_{31} : \{0 \le y \le L; \quad \sigma_0 \le \sigma \le \sigma_1; \quad \pi - \sigma_1 \le \sigma \le \pi - \sigma_0; \quad \beta = |\pi/2 - \sigma|; \quad \psi - \psi_s = \pm\pi/2\} \tag{23}$$

$$A_{32} : \{0 \le y \le L; \quad \sigma_1 < \sigma < \pi - \sigma_1; \quad \beta = |\pi/2 - \sigma|; \quad \psi - \psi_s = \pm\pi/2\} \tag{24}$$

By taking into account equations (21) to (24), one obtains the transmitted and absorbed beam flux, equations (8) and (10), as follows:

$$QT_{b,par}/E_b = \tau_{bb,1}(\theta_h) \cdot \sin\theta_z \cdot \left[S_{11} + \rho_{bb,2,b}^{\bar{n}_2}(\theta_h) \cdot \rho_{bb,1,b}^{\bar{n}_1}(\theta_h) \cdot S_{12}\right] + 2R\cos\theta_z \cdot \int_{\sigma_0}^{\sigma_1} \left[L - Y(\sigma) + \rho_{bb,2,b}(\theta_h) \cdot Y(\sigma)\right] \cdot \tau_{bb,3}(\theta) \sin\sigma d\sigma + 2R\cos\theta_z \int_0^L dy \int_{\sigma_1}^{\pi/2} \tau_{bb,3}(\theta) \cdot \rho_{bb,2,b}^{n_2(y,\sigma)}(\theta_h) \cdot \rho_{bb,1,b}^{n_1(y,\sigma)}(\theta_h) \sin\sigma d\sigma \tag{25}$$

$$QA_{b,par}/E_b = \alpha_{1,f}(\theta_h)\sin\theta_z S_1 + \tau_{bb,1}(\theta_h) \cdot \left\{\begin{matrix}\alpha_{2,b}(\theta_h) \cdot G(\bar{n}_2) + \\ \alpha_{1,b}(\theta_h) \cdot \rho_{bb,2,b}(\theta_h) \cdot G(\bar{n}_1)\end{matrix}\right\} \cdot \sin\theta_z \cdot S_{12} + 2RL\cos\theta_z \int_{\sigma_0}^{\pi/2} \alpha_{3,f}(\theta) \cdot \sin\sigma d\sigma + 2R\cos\theta_z \cdot \alpha_{2,b}(\theta_h) \cdot \int_{\sigma_0}^{\sigma_1} \tau_{bb,3}(\theta) \cdot Y(\sigma) \cdot \sin\sigma d\sigma + 2R\cos\theta_z \int_0^L dy \int_{\sigma_1}^{\pi/2} \tau_{bb,3}(\theta) \cdot \left\{\begin{matrix}\alpha_{2,b}(\theta_h) \cdot G(n_2(y,\sigma)) + \\ \alpha_{1,b}(\theta_h) \cdot \rho_{bb,2,b}(\theta_h) \cdot G(n_1(y,\sigma))\end{matrix}\right\} \cdot \sin\sigma d\sigma \tag{26}$$

Equations (16) to (20) also reduce to the following:

$$Q_{0,1,t,par}/E_b = \tau_{bd,1}(\theta_h) \cdot \sin\theta_z \cdot S_1 \tag{27}$$

$$Q_{0,1,r,par}/E_b = \tau_{bb,1}(\theta_h)\cdot\rho_{bb,2,b}(\theta_h)\cdot\rho_{bd,1,b}(\theta_h)\cdot G(\bar{n}_1)\cdot\sin\theta_z\cdot S_{12} + 2R\cos\theta_z\cdot\rho_{bb,2,b}(\theta_h)\cdot\rho_{bd,1,b}(\theta_h)\cdot\int_0^L dy\int_{\sigma_1}^{\pi/2}\tau_{bb,3}(\theta)\cdot G(n_1(y,\sigma))\cdot\sin\sigma d\sigma \quad (28)$$

$$Q_{0,2,r,par}/E_b = \tau_{bb,1}(\theta_h)\cdot\rho_{bd,2,b}(\theta_h)\cdot G(\bar{n}_2)\cdot\sin\theta_z\cdot S_{12} + 2R\cos\theta_z\cdot\rho_{bd,2,b}(\theta_h)\cdot\left\{\int_{\sigma_0}^{\sigma_1} Y(\sigma)\cdot\tau_{bb,3}(\theta)\sin\sigma d\sigma\right\} + 2R\cos\theta_z\cdot\rho_{bd,2,b}(\theta_h)\cdot\left\{\int_0^L dy\int_{\sigma_1}^{\pi/2}\tau_{bb,3}(\theta)\cdot G(n_2(y,\sigma))\cdot\sin\sigma d\sigma\right\} \quad (29)$$

$$Q_{0,3,t,par}/E_b = 2RL\cos\theta_z\cdot\int_{\sigma_0}^{\pi/2}\tau_{bd,3}(\theta)\sin\sigma d\sigma \quad (30)$$

The integrals in equations (25) to (30) do not admit analytical solutions, and therefore they are solved using numerical integration models. The Gauss quadrature integration method is used in this paper.

The reflection function (G) is given by the following relation:

$$G(n) = \begin{cases} 0, & \text{if } n \le 0 \\ \sum_{i=1}^{n}\left(\rho_{bb,1,b}\cdot\rho_{bb,2,b}\right)^{i-1} = \dfrac{1-\left(\rho_{bb,1,b}\cdot\rho_{bb,2,b}\right)^n}{1-\rho_{bb,1,b}\cdot\rho_{bb,2,b}}, & \text{if } n > 0 \end{cases} \quad (31)$$

The unknown quantities in equations (25) to (30) are given by the following relations:

$$Y(\sigma) = R\cdot(\sin\sigma - \sin\sigma_0)\tan\theta_z \quad (32)$$

$$\sin\sigma_1 = \sin\sigma_0 + L/R\cdot c\tan\theta_z \quad (33)$$

$$S_{11} = R^2(\sigma_1 - \sigma_0 + \cos\sigma_1\cdot\sin\sigma_1 - \cos\sigma_0\cdot\sin\sigma_0); \quad S_{12} = S_1 - S_{12} \quad (34)$$

$$N(y,\sigma) = \begin{cases} 0, & \text{if } N_0 < 0 \\ 1+\text{int}(N_0), & \text{if } N_0 \ge 0 \end{cases}; \quad n_1 = N/2; \quad n_2 = N - n_1 \quad (35)$$

$$N_0 = R/L\cdot(\sin\sigma - \sin\sigma_0)\cdot\tan\theta_Z - y/L \quad (36)$$

where *int()* is a function that truncates a real number to an integer one; N is the total number of reflections from surfaces A_1 and A_2; n_1 and n_2 are the number of reflections from surfaces A_1 and A_2, respectively; S_1 and S_{11} are areas of surfaces A_1 and A_{11}, respectively; Y is the y-position of a point moving on the intersection curve between surfaces A_{31} and A_{32}; y is the y-position of a point moving on surface A_3; and σ_1 is the angle that delimits surfaces A_{11} and A_{12}, (varies from 0 to $\pi/2$ radians). $\bar{N}$ and $\bar{n}$ are the

averages of N and n, respectively, over the surface portion A_{12}. These are given by the following equations:

$$\overline{N} = \begin{Bmatrix} 0, & \text{if } \overline{N}_0 < 0 \\ 1 + \text{int}(\overline{N}_0), & \text{if } \overline{N}_0 \geq 0 \end{Bmatrix}; \quad \overline{n}_1 = \overline{N}/2; \quad \overline{n}_2 = \overline{N} - \overline{n}_1 \tag{37}$$

$$\overline{N}_0 = \frac{1}{S_{12}} \int_{A_{12}} N_0(L,\sigma) \cdot ds = \{R/L \cdot \tan\theta_Z\} \cdot \left\{ \frac{4/3 \cdot \cos^3 \sigma_1}{\pi - 2\sigma_1 - \sin 2\sigma_1} - \sin\sigma_0 \right\} - 1 \tag{38}$$

3.1.2 Sun's Rays Perpendicular to the Skylight Axis

Figure 3 shows the beam light transmission through a transparent skylight when the sun's rays are perpendicular to the skylight axis. The sun's rays strike only a portion of the surface A_3. The surface portion A_{31} ($\sigma_0 \leq \sigma \leq \sigma_1$) receives the directly-transmitted flux, and the surface portion A_{32} ($\sigma_1 \leq \sigma \leq \sigma_2$) receives the transmitted-reflected flux. Only the first reflections from the skylight interior surface are considered (multiple reflections occur over a small surface near the angle σ_2).

The incident, transmitted and absorbed flux is expressed as follows:

$$Q_{per} = \int_{A_{31}} E_b \cos\theta \cdot ds + \int_{A_{32}} E_b \cos\theta \cdot ds \tag{39}$$

$$QT_{per} = QT_{b,per} + QT_{d,per} \tag{40}$$

$$QA_{per} = QA_{b,per} + QA_{d,per} \tag{41}$$

where $QT_{b,per}$ and $QT_{d,per}$ are the beam and diffuse components of the transmitted flux (QT_{per}), and $QA_{b,per}$ and $QA_{d,per}$ are the beam and diffuse components of the absorbed flux (QA_{per}). Using the same reasoning as before, the beam component flux ($QT_{b,per}$ and $QA_{b,per}$) is expressed in the following relations:

$$QT_{b,per} = \int_{A_{31}} E_b \cdot \tau_{bb,3}(\theta) \cdot \cos\theta \cdot ds + \int_{A_{32}} E_b \cdot \tau_{bb,3}(\theta) \cdot \rho_{bb,3,b}(\theta) \cdot \cos\theta \cdot ds \tag{42}$$

$$QA_{b,per} = \int_{A_3} E_b \cdot \alpha_{3,f}(\theta) \cdot \cos\theta \cdot ds + \int_{A_{32}} E_b \cdot \tau_{bb,3}(\theta) \cdot \alpha_{3,b}(\theta) \cdot \cos\theta \cdot ds \tag{43}$$

The diffuse components ($QT_{d,per}$ and $QA_{d,per}$) are given by similar relations as equations (9) and (11) with the appropriate expressions for the initial surface flux ($QT_{0,k}$):

$$Q_{0,1} = Q_{0,2} = 0 \tag{44}$$

$$Q_{0,3} = Q_{0,3,t,per} + Q_{0,3,r,per} \tag{45}$$

with:

$$Q_{0,3,t,per} = \int_{A_3} E_b \cdot \tau_{bd,3}(\theta) \cdot \cos\theta \cdot ds \tag{46}$$

$$Q_{0,3,r,per} = \int_{A_{32}} E_b \cdot \tau_{bb,3}(\theta) \cdot \rho_{bd,3}(\theta) \cdot \cos\theta \cdot ds \tag{47}$$

The surface portions A_{31} and A_{32} for the perpendicular configuration are defined as follows:

$$A_{31} : \{0 \le y \le L; \quad \sigma_0 \le \sigma \le \sigma_1\} \tag{48}$$

$$A_{32} : \{0 \le y \le L; \quad \sigma_1 < \sigma \le \sigma_2\} \tag{49}$$

where σ_1 and σ_2 are angles that delimit the surface portions A_{31} and A_{32}, given by:

$$\sigma_1 = \min(\sigma_0 + \pi - 2\theta_z, \pi - \sigma_0); \qquad \sigma_2 = \min(\pi - \theta_z, \pi - \sigma_0) \tag{50}$$

The incidence angle on the elementary surface (ds) of the surface A_3 is expressed as follows:

$$\cos\theta = \sin(\theta_z + \sigma) \tag{51}$$

By performing the integration in equations (39), (42) and (43), one obtains the following equations:

Incident flux:

$$Q_{per} = LRE_b\{\cos(\theta_z + \sigma_0) - \cos(\theta_z + \sigma_2)\} \tag{52}$$

Beam component of the transmitted flux:

$$QT_{b,per} / E_b = LR\int_{\sigma_0}^{\sigma_1} \tau_{bb,3}(\theta) \cdot \cos\theta \cdot d\sigma + LR\int_{\sigma_1}^{\sigma_2} \tau_{bb,3}(\theta) \cdot \rho_{bb,3,b}(\theta) \cdot \cos\theta \cdot d\sigma \tag{53}$$

Beam component of the absorbed flux:

$$QA_{b,per} / E_b = LR\int_{\sigma_0}^{\sigma_2} \alpha_{3,f}(\theta) \cdot \cos\theta \cdot d\sigma + LR\int_{\sigma_1}^{\sigma_2} \tau_{bb,3}(\theta) \cdot \alpha_{3,b}(\theta) \cdot \cos\theta \cdot d\sigma \tag{54}$$

Equations (46) and (47) also reduce to the following:

$$Q_{0,3,t,per} = E_b \cdot LR \int_{\sigma_0}^{\sigma_2} \tau_{bd,3}(\theta) \cdot \cos\theta \cdot d\sigma \tag{55}$$

$$Q_{0,3,r,per} = E_b \cdot LR \int_{\sigma_1}^{\sigma_2} \tau_{bb,3}(\theta) \cdot \rho_{bd,3}(\theta) \cdot \cos\theta \cdot d\sigma \tag{56}$$

3.1.3 Sun's Rays at an Arbitrary Position

Calculation of the transmitted and absorbed flux at an arbitrary solar azimuth angle is very complex to perform since it is not straightforward to find mathematically well-defined exposed surfaces using the ray tracing method. Rather, one opts to use a weighting factor to calculate the transmitted and absorbed flux based on the ones previously calculated for the sun's ray positions parallel and perpendicular to the skylight axis. Figure 4 shows the position of the skylight with respect to the sun and the four cardinal directions.

For a given skylight orientation (ψ_0), the incident flux and the weighted transmitted and absorbed flux are expressed as follows:

$$Q_{vault} = \int_{A_1} E_b \cos\theta \cdot ds + \int_{A_3} E_b \cos\theta \cdot ds \tag{57}$$

$$QT_{vault}(\theta_z, \psi_s) = QT_{b,par}(\theta_z) \cdot W + QT_{b,per}(\theta_z) \cdot [1 - W] + QT_d(\theta_z, \psi_s) \tag{58}$$

$$QA_{vaut}(\theta_z, \psi_s) = QA_{b,par}(\theta_z) \cdot W + QA_{b,per}(\theta_z) \cdot [1 - W] + QA_d(\theta_z, \psi_s) \tag{59}$$

where W is the weighting factor to be determined, and QT_d and QA_d are the diffuse components of the transmitted and absorbed flux for the arbitrary sun's rays position. The diffuse flux (QT_d and QA_d) is obtained by equations (9) and (11) by substituting the corresponding initial flux ($Q_{0,k}$, k = 1 to 3) for the arbitrary sun's rays position. The latter flux includes terms that can be integrated over the skylight surface (diffuse direct transmission terms) and terms that cannot be easily obtained (diffuse inter-reflection terms). One may use the weighting factor approach to compute the diffuse inter-reflected initial flux as follows:

$$Q_{0,k,r} = W \cdot Q_{0,k,r,par} + [1 - W] \cdot Q_{0,k,r,per}; \qquad k = 1 \text{ to } 3 \tag{60}$$

The diffuse initial exiting flux for the arbitrary sun's rays position is then expressed as follows:

$$Q_{0,1} = \int_{A_1} E_b \cdot \tau_{bd,1}(\theta) \cdot \cos\theta \cdot ds + Q_{0,1,r} \tag{61}$$

$$Q_{0,2} = Q_{0,2,r} \tag{62}$$

$$Q_{0,3} = \int_{A_3} E_b \cdot \tau_{bd,3}(\theta) \cdot \cos\theta \cdot ds + Q_{0,3,r} \tag{63}$$

Equations (57), (61) and (63) can be reduced to the following:

$$Q_{vault} / E_b = LR\{\cos\theta_z(\cos\sigma_0 - \cos\sigma_t) + \sin\theta_z(\sin\sigma_0 - \sin\sigma_t)\cos(\psi_s - \psi_t)\} + S_1 \cdot \sin\theta_z\left|\cos(\psi_s - \psi_0)\right| \tag{64}$$

$$Q_{0,1} = S_1 \cdot \tau_{bd,1}(\theta_h)\sin\theta_z\left|\cos(\psi_s - \psi_0)\right| + Q_{0,1,r} \tag{65}$$

$$Q_{0,3} = RL\int_{\sigma_0}^{\sigma_t} E_b \cdot \tau_{bd,3}(\theta) \cdot \cos\theta \cdot d\sigma + Q_{0,3,r} \tag{66}$$

where σ_t and ψ_t are the position and surface azimuth angles that correspond to the sun's rays tangent to, or reaching the boundary of the skylight surface A_3 when the sun's rays are at an arbitrary position (note that $\sigma_t = \sigma_2$ when the sun's rays are perpendicular to the skylight axis).

The incidence angle θ in equation (66) is still given by equation (2) by substituting the inclination angle β by $|\pi/2 - \sigma|$. The tangent angles (σ_t, ψ_t) are given by:

$$\sigma_t = \min\left(\pi + \tan^{-1}[\tan\theta_z \cdot \cos(\psi_s - \psi_t)],\ \ \pi - \sigma_0\right) \tag{67}$$

$$\cos(\psi_s - \psi_t) = \begin{cases} -\sin(|\psi_s - \psi_0|), & \text{if } 0 \le |\psi_s - \psi_0| \le \pi \\ \sin(|\psi_s - \psi_0|), & \text{if } \quad |\psi_s - \psi_0| > \pi \end{cases} \tag{68}$$

The weighting function W can be determined by calculating the incident flux on the skylight surface A_3 ($Q_{i,3}$) at an arbitrary solar azimuth angle, and the incident flux for the parallel and perpendicular sun's ray positions ($Q_{i,3,par}$ and $Q_{i,3,per}$). The function W can, thus, be expressed as follows:

$$W = \frac{Q_{i,3} - Q_{i,3,per}}{Q_{i,3,par} - Q_{i,3,per}} \tag{69}$$

By taking into account equations (5), (52) and (64), one obtains the following relation for the weighting function W:

$$W = \frac{\cos(\theta_z + \sigma_2) - \cos\theta_z\cos\sigma_t + \sin\theta_z\{\sin\sigma_0 + [\sin\sigma_0 - \sin\sigma_t]\cos(\psi_s - \psi_t)\}}{\cos(\theta_z - \sigma_0) + \cos(\theta_z + \sigma_2)} \tag{70}$$

3.1.4 Beam Optical Characteristics

The above analysis shows that all the parameters needed to calculate the skylight overall transmittance, absorptance and reflectance are now available. These are expressed as follows:

$$\tau_{vault} = \frac{QT_{vault}}{Q_{vault}}; \quad \alpha_{vault} = \frac{QA_{vault}}{Q_{vault}}; \quad \rho_{vault} = 1 - \tau_{vault} - \alpha_{vault} \tag{71}$$

3.1.5 Beam Equivalent Optical Characteristics

Introducing the concept of the optically equivalent flat skylight that has the same aperture surface area and yields the same transmitted, absorbed and reflected flux as the barrel vault skylight, the equivalent optical characteristics of barrel vault skylights are expressed as follows[3, 14]:

$$\tau_{eq}(\theta_z, \psi_s) = \tau_{vault}(\theta_z, \psi_s) \cdot \varepsilon(\theta_z, \psi_s) \tag{72}$$

$$\alpha_{eq}(\theta_z, \psi_s) = \alpha_{vault}(\theta_z, \psi_s) \cdot \varepsilon(\theta_z, \psi_s) \tag{73}$$

$$\rho_{eq}(\theta_z, \psi_s) = \rho_{vault}(\theta_z, \psi_s) \cdot \varepsilon(\theta_z, \psi_s) \tag{74}$$

where ε is the ratio of the incident flux on the skylight surface to that incident on the optically-equivalent flat surface, given by:

$$\varepsilon(\theta_z, \psi_s) = Q_{vault} / (E_b S_h \cos\theta_z) \tag{75}$$

Substituting equation (64) in equation (75), one obtains the following equation:

$$\begin{aligned} \varepsilon(\theta_z, \psi_s) = R/(2L\cos\sigma_0) \cdot (\pi/2 - \sigma_0 - \cos\sigma_0 \sin\sigma_0) \cdot |\cos(\psi_s - \psi_0)| \cdot \tan\theta_z + \\ \{\cos\sigma_0 - \cos\sigma_t + (\sin\sigma_0 - \sin\sigma_t) \cdot \tan\theta_z \cdot \cos(\psi_s - \psi_t)\}/(2\cos\sigma_0) \end{aligned} \tag{76}$$

It should be noted that the equivalent skylight optics (τ_{eq}, ρ_{eq}, α_{eq}) may become infinite when the sun is at the horizon ($\theta_z = \pi/2$) since the incident flux ratio (ε) may tend to infinity. This means that vault skylights may outperform flat skylights with similar glazing when the sun is at low altitude angles. This performance feature actually depends on the shape geometry characteristics (truncation angle and length-to-radius ratio). For example, low profile skylights (truncation angle σ_0 close to $\pi/2$) may yield similar performance as flat skylights since ε tends to 1.

3.2 Diffuse Light Transmission

Consider a skylight receiving light from a diffuse source. Any ray emanating from the source undergoes a direct transmission through the skylight surface and a series of inter-reflections from the skylight interior surface. The directly transmitted and the inter-reflected components are both dependent on the source itself and the transparency of the glazing. For partially diffusing glazing, any source ray undergoes both direct transmission and inter-reflection. However, for transparent glazing, any source ray may undergo

both direct transmission and inter-reflection, or only inter-reflection. The inter-reflected flux may be assumed diffuse. Figure 5 shows the diffuse light transmission process through a vault skylight.

The incident diffuse flux on a vault skylight is expressed as follows:

$$Q_{d,vault} = \sum_{k=1}^{3} Q_{i,k} = \sum_{k=1}^{3} \int_{A_k} E_{d,t} \cdot ds \tag{77}$$

where $Q_{i,k}$ is the incident flux on surface A_k, and $E_{d,t}$ is the diffuse illuminance on a tilted surface.

By using the net radiation method, one obtains the surface inter-reflected flux (Q_k) as follows:

$$Q_1 = \rho_{d,1,b}\left[F_{12}Q_2 + F_{31}Q_3 + (1-c_1)(1-\bar{\gamma}_2 F_{1b})Q_{t,2} + c_3(1-\bar{\gamma}_3 F_{3b})Q_{t,3}\right] \tag{78}$$

$$Q_2 = \rho_{d,2,b}\left[F_{12}Q_1 + F_{31}Q_3 + (1-c_1)(1-\bar{\gamma}_1 F_{1b})Q_{t,1} + c_3(1-\bar{\gamma}_3 F_{3b})Q_{t,3}\right] \tag{79}$$

$$Q_3 = \frac{\rho_{d,3,b}}{(1-\rho_{d,3,b}F_{33})}\begin{bmatrix} F_{13}(Q_1+Q_2) + c_1(1-\bar{\gamma}_1 F_{1b})Q_{t,1} + \\ c_1(1-\bar{\gamma}_2 F_{1b})Q_{t,2} + (1-2c_3)(1-\bar{\gamma}_3 F_{3b})Q_{t,3} \end{bmatrix} \tag{80}$$

where $Q_{t,k} = \tau_{d,k}Q_{i,k}$ is the diffuse transmitted flux through surface A_k; Q_k is the inter-reflected flux from surface A_k; c_1 and c_3 are coefficients to be determined for surfaces A_1 (or A_2) and A_3, respectively; F_{kj} is a view factor of surface A_k to surface A_j ; F_{kb} is a view factor of surface A_k to the skylight base surface; $\bar{\gamma}_k$ is the average value of γ_k over surface A_k, to be determined; $\tau_{d,k}$ is the diffuse transmittance of surface A_k; and $\rho_{d,k,b}$ is the diffuse back reflectance of surface A_k.

The Appendix presents methods to compute the coefficients γ_1, γ_2 and γ_3 and their surface averages. The coefficients c_1 and c_3 take into account the diffuse components of the surface transmitted flux ($Q_{t,k}$) that does not reach the skylight base surface. These are given by:

$$c_1 = F_{13}/(1-F_{1b}); \qquad c_3 = F_{31}/(1-F_{3b}) \tag{81}$$

The transmitted, and absorbed flux is then given by the following equations:

$$QT_{d,vault} = \sum_{k=1}^{3}\left(\bar{\gamma}_k F_{kb}\tau_{d,k}Q_{i,k} + F_{kb}Q_k\right) \tag{82}$$

$$QA_{d,vault} = \sum_{k=1}^{3}\left\{\alpha_{d,k,f}Q_{i,k} + \alpha_{d,k,b}/\rho_{d,k,b}\cdot Q_k\right\} \tag{83}$$

where $\alpha_{d,k,f}$ and $\alpha_{d,k,b}$ are the front and back diffuse absorptances of surface A_k, $\rho_{d,k,f}$and $\rho_{d,k,b}$ are the front and back diffuse reflectances of surface A_k, and $\tau_{d,k}$ is the diffuse transmittance of surface A_k.

It should be noted that the transmitted and absorbed flux (equations 82 and 83) for diffuse light is dependent on the skylight geometry, the optical properties of the skylight component surfaces, the incident flux on the skylight component surfaces ($Q_{i,k}$), and the glazing transparency of the skylight component surfaces (accounted for by the coefficients $\overline{\gamma}_k$) . For surfaces with translucent glazing, the coefficients $\overline{\gamma}_k$ = 1 independently of the light source. However, for surfaces with transparent glazing, the coefficients $\overline{\gamma}_k$ = 0 for the ground-reflected light, and are given by equations (126) and (134) of the Appendix.

3.2.1 Diffuse Optical Characteristics

The diffuse optical characteristics for a given diffuse light source are expressed as follows:

$$\tau_{d,vault} = \frac{QT_{d,vault}}{Q_{d,vault}}; \quad \alpha_{d,vault} = \frac{QA_{d,vault}}{Q_{d,vault}}; \quad \rho_{d,vault} = 1 - \tau_{d,vault} - \alpha_{d,vault} \tag{84}$$

3.2.2 Diffuse Equivalent Optical Characteristics

Two models are used to compute the equivalent optical characteristics under a diffuse sky light: luminance-based and illuminance-based models. In the luminance-based model, the sky luminance pattern is known (e.g., standard sky conditions), whereas in the illuminance-based model the illuminance on a horizontal surface is known. The luminance-based model is more accurate and results in more calculation time than the illuminance-based model. The latter model is more suitable to calculate the annual performance of skylights such as lighting energy savings.

3.2.2.1 Luminance-Based Model

This approach treats each luminous point in the sky as a beam source. The equivalent optical characteristics for the beam light are given by equations (72) to (74). The hemispherical values of the equivalent optical characteristics are then obtained by integrating over the sky vault. However, the ground-reflected light is treated as in the upcoming section, equations (94) to (96).

The diffuse equivalent optical characteristics are given by:

$$\tau_{eq,d} = \frac{1}{E_{dh}} \int_{\eta=0}^{\eta=\pi/2} \int_{\phi=-\pi}^{\phi=\pi} \tau_{eq}(\eta, \psi_s - \phi) \cdot \Gamma(\eta, \theta_z, \phi) \cdot \cos\eta \cdot \sin\eta \cdot d\eta \cdot d\phi + \tau_{d,vault}(\overline{\gamma}_{1,gr}, \overline{\gamma}_{2,gr}, \overline{\gamma}_{3,gr}) \cdot \varepsilon_{d,gr} \tag{85}$$

$$\alpha_{eq,d} = \frac{1}{E_{dh}} \int_{\eta=0}^{\eta=\pi/2} \int_{\phi=-\pi}^{\phi=\pi} \alpha_{eq}(\eta, \psi_s - \phi) \cdot \Gamma(\eta, \theta_z, \phi) \cdot \cos\eta \cdot \sin\eta \cdot d\eta \cdot d\phi + \alpha_{d,vault}(\overline{\gamma}_{1,gr}, \overline{\gamma}_{2,gr}, \overline{\gamma}_{3,gr}) \cdot \varepsilon_{d,gr} \tag{86}$$

$$\rho_{eq,d} = \frac{1}{E_{dh}} \int_{\eta=0}^{\eta=\pi/2} \int_{\phi=-\pi}^{\phi=\pi} \rho_{eq}(\eta, \psi_s - \phi) \cdot \Gamma(\eta, \theta_z, \phi) \cdot \cos\eta \cdot \sin\eta \cdot d\eta \cdot d\phi + \rho_{d,vault}(\overline{\gamma}_{1,gr}, \overline{\gamma}_{2,gr}, \overline{\gamma}_{3,gr}) \cdot \varepsilon_{d,gr} \tag{87}$$

where $\Gamma(\eta,\theta_z,\phi)$ is the luminance at a given sky point, defined by the point zenithal angle (η) and its relative azimuth angle with respect to the sun position (ϕ), and E_{dh} is the diffuse horizontal illuminance, given by the following equation:

$$E_{dh} = \int_{\eta=0}^{\eta=\pi/2} \int_{\phi=-\pi}^{\phi=\pi} \Gamma(\eta,\theta_z,\phi) \cdot \cos\eta \cdot \sin\eta \cdot d\eta \cdot d\phi \tag{88}$$

3.2.2.2 Illuminance-Based Model

Vault skylights receive sky diffuse light as well as surrounding/ground-reflected light. The incident total flux on the vault skylight surface is expressed as follows:

$$Q_{d,vault} = \int_{A_{vault}} E_{gr} ds + \int_{A_{vault}} E_{sky} ds \tag{89}$$

where E_{gr} is the illuminance from the ground received on the elemental surface (ds), and E_{sky} is the illuminance from the sky received on the elemental surface (ds).

The sky luminous flux may be decomposed into three components: a background uniform flux, circumsolar flux and horizon brightening flux[17]. For translucent glazing, the surrounding/ground-reflected flux and the three components of the sky luminous flux undergoes both direct transmission and inter-reflections. For transparent glazing, however, the ground-reflected and horizon brightening flux undergoes only inter-reflections. The circumsolar flux is treated as beam light. Equation (89) reads as follows:

$$Q_{d,vault} = \int_{A_{vault}} (E_{gr} + E_{su} + E_{hb}) ds + \int_{A_{vault}} E_{cs} \cos\theta \cdot ds \tag{90}$$

where E_{su} is the illuminance from the uniform background sky component received on the elemental surface (ds), E_{hb} is the illuminance from the horizon brightening sky component received on the elemental surface (ds), and E_{cs} is the illuminance from the circumsolar sky component received on the elemental surface (ds).

The total transmitted, absorbed and reflected flux reads as follows:

$$\begin{aligned} QT_{d,vault} = {} & \tau_{d,vault,gr}(\bar{\gamma}_{1,gr},\bar{\gamma}_{2,gr},\bar{\gamma}_{3,gr}) \int_{A_{vault}} E_{gr} ds + \tau_{d,vault,hb}(\bar{\gamma}_{1,gr},\bar{\gamma}_{2,gr},\bar{\gamma}_{3,gr}) \int_{A_{vault}} E_{hb} ds + \\ & \tau_{d,vault,su}(\bar{\gamma}_{1,su},\bar{\gamma}_{2,su},\bar{\gamma}_{3,su}) \int_{A_{vault}} E_{su} ds + \tau_{vault} \int_{A_{vault}} E_{sc} \cos\theta \cdot ds \end{aligned} \tag{91}$$

$$QA_{d,vault} = \alpha_{d,vault,gr}(\bar{\gamma}_{1,gr},\bar{\gamma}_{2,gr},\bar{\gamma}_{3,gr}) \int_{A_{vault}} E_{gr} ds + \alpha_{d,vault,hb}(\bar{\gamma}_{1,gr},\bar{\gamma}_{2,gr},\bar{\gamma}_{3,gr}) \int_{A_{vault}} E_{hb} ds + \alpha_{d,vault,su}(\bar{\gamma}_{1,su},\bar{\gamma}_{2,su},\bar{\gamma}_{3,su}) \int_{A_{vault}} E_{su} ds + \alpha_{vault} \int_{A_{vault}} E_{sc} \cos\theta \cdot ds \quad (92)$$

$$QR_{d,vault} = \rho_{d,vault,gr}(\bar{\gamma}_{1,gr},\bar{\gamma}_{2,gr},\bar{\gamma}_{3,gr}) \int_{A_{vault}} E_{gr} ds + \rho_{d,vault,hb}(\bar{\gamma}_{1,gr},\bar{\gamma}_{2,gr},\bar{\gamma}_{3,gr}) \int_{A_{vault}} E_{hb} ds + \rho_{d,vault,su}(\bar{\gamma}_{1,su},\bar{\gamma}_{2,su},\bar{\gamma}_{3,su}) \int_{A_{vault}} E_{su} ds + \rho_{vault} \int_{A_{vault}} E_{sc} \cos\theta \cdot ds \quad (93)$$

For surfaces with translucent glazing $\bar{\gamma}_{k,gr}$ = $\bar{\gamma}_{k,su}$ = 1 for the ground-reflected and sky diffuse lights. For surfaces with transparent glazing, $\bar{\gamma}_{k,gr}$ = 0 for the ground-reflected and horizon-brightening lights, and $\bar{\gamma}_{k,su}$, are given by equations (126) and (134) of the Appendix for the background diffuse sky light.

The diffuse equivalent optical characteristics for the combined sky and ground-reflected light are given by:

$$\tau_{eq,d} = \tau_{d,vault,gr}(\bar{\gamma}_{1,gr},\bar{\gamma}_{2,gr},\bar{\gamma}_{3,gr}) \cdot \varepsilon_{d,gr} + \tau_{d,vault,hb}(\bar{\gamma}_{1,gr},\bar{\gamma}_{2,gr},\bar{\gamma}_{3,gr}) \cdot \varepsilon_{d,hb} + \tau_{d,vault,su}(\bar{\gamma}_{1,su},\bar{\gamma}_{2,su},\bar{\gamma}_{3,su}) \cdot \varepsilon_{d,su} + \tau_{eq} \cos\theta_z E_{cs} / E_{dh} \quad (94)$$

$$\alpha_{eq,d} = \alpha_{d,vault,gr}(\bar{\gamma}_{1,gr},\bar{\gamma}_{2,gr},\bar{\gamma}_{3,gr}) \cdot \varepsilon_{d,gr} + \alpha_{d,vault,hb}(\bar{\gamma}_{1,gr},\bar{\gamma}_{2,gr},\bar{\gamma}_{3,gr}) \cdot \varepsilon_{d,hb} + \alpha_{d,vault,su}(\bar{\gamma}_{1,su},\bar{\gamma}_{2,su},\bar{\gamma}_{3,su}) \cdot \varepsilon_{d,su} + \alpha_{eq} \cos\theta_z E_{cs} / E_{dh} \quad (95)$$

$$\rho_{eq,d} = \rho_{d,vault,gr}(\bar{\gamma}_{1,gr},\bar{\gamma}_{2,gr},\bar{\gamma}_{3,gr}) \cdot \varepsilon_{d,gr} + \rho_{d,vault,hb}(\bar{\gamma}_{1,gr},\bar{\gamma}_{2,gr},\bar{\gamma}_{3,gr}) \cdot \varepsilon_{d,hb} + \rho_{d,vault,su}(\bar{\gamma}_{1,su},\bar{\gamma}_{2,su},\bar{\gamma}_{3,su}) \cdot \varepsilon_{d,su} + \rho_{eq} \cos\theta_z E_{cs} / E_{dh} \quad (96)$$

The illuminance on a tilted surface is evaluated for different sky conditions:

For the ground-reflected light[16]:

$$E_{gr} / E_{dh} = \rho_{gr} \cdot E_{gh} / E_{dh} \cdot (1 - \cos\beta)/2 \quad (97)$$

For the isotropic overcast skies[16]:

$$E_{su} / E_{dh} = (1 + \cos\beta)/2 \quad (98)$$

For the CIE standard overcast skies[18, 19]:

$$E_{su} / E_{dh} = \frac{3}{14}(1 + \cos\beta) + \frac{4}{7\pi}\{\sin\beta + (\pi - \beta)\cos\beta\} \quad (99)$$

For the anisotropic diffuse skies[17]:

$$E_{su} / E_{dh} = (1 - F_1)(1 + \cos\beta)/2 \quad (100)$$

$$E_{cs} / E_{dh} = F_1 / C \tag{101}$$

$$E_{hb} / E_{dh} = F_2 \cdot \sin\beta \tag{102}$$

$$C = \max(0.087\ , \cos\theta_z) \tag{103}$$

where E_{gh} is the global illuminance on a horizontal surface, ρ_{gr} is the ground/surroundings reflectance, and F_1 and F_2 are coefficients for the circumsolar and horizon brightening components of the Perez et al. model[17], respectively.

The diffuse incident flux on the skylight surfaces and the diffuse flux ratio ε_d are evaluated for different light sources and sky conditions:

For the ground-reflected light,

$$Q_{i,1,gr} = Q_{i,2,gr} = \frac{1}{2}\rho_{gr} E_{gh} S_1 \tag{104}$$

$$Q_{i,3,gr} = \frac{1}{2}\rho_{gr} E_{gh} (S_3 - S_h) \tag{105}$$

$$\varepsilon_{d,gr} = \rho_{gr} \frac{E_{gh}}{2E_{dh}} (1/F_{sb} - 1) \tag{106}$$

For the isotropic overcast skies (E_{cs} = E_{hb} = 0),

$$Q_{i,1,su} = Q_{i,2,su} = E_{dh} S_1 / 2 \tag{107}$$

$$Q_{i,3,su} = E_{dh} (S_3 + S_h) / 2 \tag{108}$$

$$\varepsilon_{d,su} = (1/F_{sb} + 1)/2 \tag{109}$$

For the CIE standard overcast skies (E_{cs} = E_{hb} = 0),

$$Q_{i,1,su} = Q_{i,2,su} = E_{dh} S_1 \left(\frac{3}{14} + \frac{4}{7\pi} \right) \tag{110}$$

$$Q_{i,3,su} = E_{dh} \left\{ \frac{3}{14} S_3 + S_h \left(\frac{1}{2} + \frac{4\sigma_0}{7\pi} + \frac{8}{7\pi} (1 - \sin\sigma_0) / \cos\sigma_0 \right) \right\} \tag{111}$$

$$\varepsilon_{d,su} = 1/2 + \frac{1}{7}(3 + 8/\pi) S_1 / S_h + \frac{3}{14} S_3 / S_h + 4\sigma_0 / (7\pi) + \frac{8}{7\pi} (1 - \sin\sigma_0) / \cos\sigma_0 \tag{112}$$

For the anisotropic skies,

$$Q_{i,1,su} = Q_{i,2,su} = E_{dh}(1-F_1)S_1/2 \tag{113}$$

$$Q_{i,1,hb} = Q_{i,2,hb} = S_1 \cdot F_2 \cdot E_{dh} \tag{114}$$

$$Q_{i,3,su} = E_{dh}(1-F_1)(S_3+S_h)/2 \tag{115}$$

$$Q_{i,3,hb} = S_h E_{dh} F_2 (1-\sin\sigma_0)/\cos\sigma_0 \tag{116}$$

$$\varepsilon_{d,su} = (1-F_1)(1/F_{sb}+1)/2 \tag{117}$$

$$\varepsilon_{d,hb} = 2F_2 S_1/S_h + F_2(1-\sin\sigma_0)/\cos\sigma_0 \tag{118}$$

where S_k is the area of surfaces A_k (k=1 to 3), and F_{sb} is the view factor of the skylight surface to its base surface. These are given by the following relations:

$$S_1 = S_2 = R^2(\pi/2 - \sigma_0 - \cos\sigma_0 \cdot \sin\sigma_0); \quad S_3 = RL \cdot (\pi - 2\sigma_0); \quad S_h = 2RL \cdot \cos\sigma_0 \tag{119}$$

$$F_{sb} = S_h/(2S_1+S_3) = \frac{2\cos\sigma_0}{(\pi-2\sigma_0)(1+R/L) - R/L \cdot \sin 2\sigma_0} \tag{120}$$

4 Experimental Procedure

Non-flat (or projecting) skylights exhibit different performance than planar fenestration[1-3]. One of the most important parameters of skylights are their optical properties. Skylight optical properties are not only important for product rating, but also for daylighting and energy performance predictions. Contrary to planar fenestration, there is no standard procedure to measure the skylight optical properties under laboratory or real settings. For example, the ASTM Standard E972-96[20] (or E1084-86/96[21]) to measure the transmittance of flat sheets of glazing under sunlight cannot be used for projecting skylights for a number of reasons. One main reason is that the use of one illuminance sensor underneath the glazing is not adequate to calculate the transmitted energy through the skylight, especially for large skylight apertures. Furthermore, due to the forming process of skylight glazing, the skylight surface may exhibit a variable thickness, and therefore variable local transmittance (for example, some surface points may exhibit lens effects). This effect may result in the misrepresentation of the overall performance. In addition, skylights transmit light not only by direct transmission, but also by inter-reflection within the inside surfaces of the skylight. Capturing the inter-reflected energy needs some sensors placed close to the bottom surface of the skylight.

Recognizing this gap in skylight performance measurements, we adopted an experimental procedure to measure the skylight visible transmittance under real sky conditions. Several skylight shapes, from which a barrel vault skylight, were tested. The purpose of the measurements was to validate the predictions of the SkyVision computer tool.

A rectangular wooden box was erected as a scale model of a simple commercial building, and was placed on the roof of a building in Ottawa (latitude = 45.32^o north, and longitude = 75.67^o east), Ontario, Canada. The box measured 2.32 m (91.5") length x 1.73 m (68") width x 1.22 m (48") height, and was oriented towards the southwest with an angle of 62^o from the south cardinal direction. The top surface of the box was fitted with a curbed opening to accommodate the skylights to be tested. The barrel vault skylight had the following dimensions: length = 1.18 m, radius = 0.286 m, truncation angle $\sigma_0 = 0^0$. The end surfaces of the skylight (A_1 and A_2) were 13 mm single clear polycarbonate glazing with sheet normal transmittance = 0.79 and reflectance = 0.08. The top surface (A_3) was 3 mm single clear polycarbonate glazing with sheet normal transmittance = 0.86 and reflectance = 0.087. The optical properties of the glazing sheets the skylight was made of were taken from the glazing database of the Optics program[22], version 5.1.

The equivalent visible transmittance of the skylight (τ_{eq}), is defined as the ratio of the transmitted energy flux exiting from the skylight aperture opening to the flux incident on the horizontally projected skylight surface. To measure the transmitted energy flux, five illuminance sensors were placed at the skylight base surface, one in the center and one on each side between the center and the edge of the skylight. The sensor spacing was chosen so that each sensor represented the same surface area. To avoid any significant reflected light back to the skylight inside surfaces, black fabric was dropped from the edges of the skylight to the floor surface of the box. The five sensors were placed on a black wooden support. Figure 6 shows a schematic description of the measurement setup and sensor positions.

The outdoor solar radiation and illuminance were measured at the rooftop permanent weather station using a YANKEE SDR-1 radiometer. The YANKEE had two sensors for the solar irradiance and illuminance measurement. An automatic controlled shadow band periodically passed over the sensors in order to measure the diffuse horizontal irradiance and illuminance. When the band was removed from the sensor, global horizontal irradiance and illuminance measurements were taken.

The illuminance sensors were of type LI-COR model LI-210SA. The sensors were cosine corrected up to an incidence angle of 80^o, and had a sensitivity response function within 5% of the CIE Vλ photometric efficiency function. All the illuminance sensors were calibrated by the manufacturer against an Eppley Precision Spectral Pyranometer. However, as part of our quality assurance procedure, all illuminance sensors were checked at our laboratory by comparing their readings with a calibrated hand-held illuminance meter. Sensors whose readings deviated by more than their uncertainty limit from the hand-held illuminance meter were not used in the experiment. As stated by the manufacture, the maximum calibration uncertainty was about 5% within the sensor sensitivity range (from an incidence angle of 0^o to

80°; the error is very large beyond this angle). The YANKEE radiometer was calibrated by the manufacturer. The YANKEE calibration was also checked by comparing its readings with an outdoor LI-COR sensor. Given the definition of the measured equivalent visible transmittance, the maximum uncertainty in the measurement of the equivalent visible transmittance was calculated to be $\sqrt{2}$ x 5% = 7% within the sensor sensitivity range.

The illuminance sensors were connected to a data acquisition system. The solar radiation radiometers were connected to a separate data acquisition system of the permanent weather station. Each data acquisition system was connected to a personal computer, which ran the data acquisition program. The sensor signals were collected and sent to the personal computer in voltage unit, which were then transformed to the desired units using the sensor calibration curves supplied by the sensor manufacturers. The sampling rate of the data acquisition systems was fixed at one minute, and sensor readings were averaged over a five-minute interval. The measurements were conducted over a whole day period, thereby covering different sky conditions: overcast, partly cloudy and clear sunny skies. Measurements under rainy or foggy days were discarded. The measurement results were presented for each sensor averaged-reading on a five-minute time step. More details may be found in this web site: http://irc.nrc-cnrc.gc.ca/ie/light/skyvision/publications.html[23].

5 Results and Discussion

The previously developed models are first compared with actual measurements. Then, the models are applied to predict the beam equivalent visible transmittance for a barrel vault skylight at various incidence and azimuth angles compared to a flat skylight with similar glazing. Finally, predictions of the diffuse equivalent visible transmittance of a barrel vault skylight using the luminance-based and illuminance-based models are compared. The luminance-based and illuminance-based models use the models of Perez et al.[24, 17] to predict the sky luminance pattern and horizontal illuminance, respectively, based on the weather data for the location under consideration.

5.1 Model Validation

Figure 7 shows a comparison between the measured and predicted equivalent visible transmittance of a clear barrel vault skylight for the combined sky and sunbeam light on October 24, 2003. The sky conditions were partly cloudy in the morning and mostly sunny in the afternoon. The profiles of the horizontal diffuse and global (beam plus diffuse) illuminance are also plotted in the figure. The luminance-based model was used to predict the diffuse transmittance of the skylight. The illuminance-based model also gave approximately the same results as the luminance-based model. The measured transmittance varied about 12% around the daily average. The minimum transmittance occurred when the sunbeam light was almost parallel to the main axis of the skylight. Given the measurement uncertainty of 7%, the model predictions followed the same trend, and were in good agreement with the measurements, with a

maximum difference of about 11%. This difference may be attributed to the five sensors of not being adequate to cover the large skylight opening and to accurately measure the transmitted energy.

5.2 Skylight Visible Transmittance Profile

A barrel vault skylight with a length-to-radius ratio L/R = 4 and a truncation angle $\sigma_0 = 0$ is considered as an example application. The skylight surfaces have uniform glazing. Two types of glazing are considered: transparent with a double clear glass (with pane optical properties at normal incidence angle $\tau = 0.88$, $\rho_f = \rho_b = 0.08$), and fully translucent glazing with similar diffuse optical properties as the double clear glass ($\tau_d = 0.70$, $\rho_{d,f} = \rho_{d,b} = 0.22$). For the transparent glazing, the transmittance and reflectance at oblique incidence angles are calculated using the laws of optics. The models are also used to predict the daily profile of the diffuse transmittance during typical summer and winter days in the Ottawa region (latitude = 45°), Ontario, Canada. Three types of standard sky conditions are considered: CIE standard overcast[25], IES partly cloudy[26] and CIE standard clear[25] as well as weather-based dynamic sky conditions[17, 23]. The ground reflectance is given a value of $\rho_{gr} = 0.2$ for summer days, and 0.6 for winter days (snow-covered ground).

5.2.1 Beam Equivalent Visible Transmittance Profile

Figure 8 shows the profiles of the equivalent transmittance (τ_{eq}) for translucent and transparent skylights as a function of the incidence angle on a horizontal surface for a number of skylight relative azimuth angles ($|\psi_s - \psi_0| = 0°$, 45° and 90°). The transmittance profile of a flat skylight with similar glazing is also plotted in the figure. Vault skylights may transmit substantially more beam light when the sun's rays are perpendicular to the skylight axis ($|\psi_s - \psi_0| = 90°$) than when the sun's rays are parallel to the skylight axis ($|\psi_s - \psi_0| = 0°$), particularly at high incidence angles (e.g., winter days). Transparent vaults transmit up to 75% more beam light than translucent vaults for incidence angles $\theta_z < 75°$ (e.g., summer days). As compared with flat skylights with similar glazing, transparent vaults transmit substantially more beam light at high incidence angles (i.e., low sun altitudes). For instance, at an incidence angle $\theta_z = 70°$ (e.g., winter days at noontime), transparent vaults may transmit up to 70% more beam light than flat transparent skylights. At near normal incidence angles (e.g., summer days at noontime), transparent vaults transmit approximately the same amount as their counterpart flat skylights. However, translucent vaults transmit up to 40% less beam light than translucent flat skylights for incidence angles $\theta_z < 65°$. In this regard, transparent vaults out-perform flat skylights with similar glazing, particularly in regions with high latitudes such as Ottawa. Furthermore, translucent vaults would be a better option than flat translucent skylights to reduce solar heat gains in summer while they provide the same illumination levels at winter times.

5.2.2 Diffuse Equivalent Visible Transmittance Profile

Figure 9 shows the hourly profiles of the diffuse equivalent transmittance ($\tau_{eq,d}$) for fully translucent and transparent vault skylights during a typical summer day (21 June). The results are obtained using the luminance-based model for a skylight oriented towards the east direction ($\psi_0 = -90^o$). The sky condition does not significantly affect the diffuse transmittance of transparent skylights (maximum difference is about 6%, which is attributed mostly to the ground-reflected light on sunny days). When compared with flat transparent skylights (transmittance = 0.70), transparent vaults transmit up to 18% more diffuse light. However, the sky condition does affect the diffuse transmittance of translucent vaults mostly through the ground-reflected light, which is more pronounced during sunny days. Translucent vaults transmit up to 35% more diffuse light under sunny days than under overcast days. Furthermore, under sunny days, translucent vaults transmit as much diffuse light as transparent vaults. When compared with flat translucent skylights, translucent vaults transmit about 16% less diffuse light under overcast sky conditions, and transmit about 14% more diffuse light under clear sky conditions.

Figure 10 shows the hourly profiles of the diffuse equivalent transmittance ($\tau_{eq,d}$) for translucent and transparent vault skylights during a typical winter day (21 December). The results are obtained using the luminance-based model for a skylight oriented towards the east direction ($\psi_0 = -90^o$). The sky condition slightly affects the diffuse transmittance of transparent skylights (maximum difference is about 15%, which is attributed mostly to the ground-reflected light on sunny days). When compared with flat transparent skylights, transparent vaults transmit about 30% more diffuse light. However, the sky condition significantly affects the diffuse transmittance of translucent vaults through the ground-reflected light, which is more pronounced during sunny days. Translucent vaults transmit up to 70% more diffuse light under sunny days than under overcast days. Furthermore, under sunny days, translucent vaults transmit about 20% more diffuse light than transparent vaults. When compared with flat translucent skylights, translucent vaults transmit about 6% less diffuse light under overcast sky conditions, and transmit about 60% more diffuse light under clear sky conditions.

5.3 Luminance-Based Versus Illuminance-Based Model Comparison

Figures 11 and 12 show the profiles of the diffuse transmittance of transparent and translucent vault skylights predicted by the luminance-based and illuminance-based models under dynamic sky conditions during typical sunny days in summer (28 June) and winter (28 December), respectively. The physical properties of the simulated skylight are the same as those in section 5.2. The luminance-based model uses the model of Perez et al.[24] while the illuminance-based model uses the other model of Perez et al.[17]. Both Perez et al. models use inputs from a weather data file. On the 28th of December, the ground is covered by snow. Under sunny days in summer/winter, both prediction models yield approximately the same results, except at the sun rise/set hours where the illuminance-based model slightly over/under predicts the diffuse transmittance due to the fact that the coefficients (F_1 and F_2) of the Perez et al.[17]

model are subject to high uncertainty when the circumsolar light is close to the horizon-brightening light ($\theta_z \approx 85°$). This comparison demonstrates the equivalency of both prediction models under the given conditions.

6 Conclusions

This paper deals with the development of prediction models to compute the optical characteristics of barrel vault skylights under beam and diffuse light. The models are based on the ray-tracing technique, and can handle vault skylights with different shapes (low or high profiles), sizes (long or short) and glazing types (multi-pane partially-diffusing, or clear). Two types of models were developed to compute the skylight optical characteristics under diffuse light: luminance-based and illuminance-based. The luminance-based model, which is used when the sky relative luminance distribution pattern is known, is more accurate, but takes more calculation time than the illuminance-based model, which is used when the outdoor horizontal illuminance is instead known. Actual measurements of the skylight visible transmittance under sunlight were conducted to validate the prediction models. The model predictions for a clear barrel vault skylight compared reasonably well with the actual measurements. Application of the models to a high profile skylight with length-to-radius ratio L/R = 4 showed that transparent vault skylights are more effective than flat skylights with similar glazing in boosting the transmittance for beam light, particularly in winter days. Translucent vault skylights are more effective than translucent flat skylights to reduce solar heat gains in summer while providing the same illumination levels at winter times. Under sunny days, the ground-reflected light has a significant impact on the skylight transmittance, particularly for translucent vault skylights. Under sunny days, translucent vault skylights may transmit up to 20% more diffuse light than transparent vault skylights, particularly in winter times. However, under overcast days, translucent vault skylights may transmit up to 25% less diffuse light than transparent vault skylights, particularly in summer times. The predictions from the luminance-based and illuminance-based models showed good agreement with each other. Therefore, the simpler and faster illuminance-based model may be used with acceptable accuracy, particularly for annual performance calculation.

ACKNOWLDGEMENTS

This work was funded by the Institute for Research in Construction of the National Research Council of Canada, PERD (Panel on Energy Research and Development), Natural Resources of Canada (Buildings Group), and Public Works and Government Services of Canada. The author is very thankful for their contribution. The author would also like to extend his gratitude to Dr. Guy Newsham (Lighting group, IRC/NRCC) for his constructive comments on the paper.

7 References

1 Laouadi, A. Design with SkyVision: a computer tool to predict daylighting performance of skylights. Proceedings of the CIB World Building Conference, Toronto. Ontario: National Research Council of Canada, May 2004.

2 McHugh J., Dee R., and Saxena M. Visible light transmittance of skylights. PIER Report No. 400-99-013, California Energy Commission, 2004.

3 Laouadi A., and Atif M.R. Prediction model of optical characteristics for barrel vault skylights. Journal of Illuminating Engineering Society of North America, 2002; 31(2): 52-65.

4 Klems J.K., Solar heat gain through a skylight in a light well. ASHRAE Transactions, 2003; 109(1). 1-8

5 Laouadi, A., Atif, M.R. and Galasiu, A.D. Towards developing skylight design tools for thermal and energy performance of atriums in cold climates. Building and Environment, 2002: 37(12). 1289-1316.

6 Hechong Mahone Group (HMG). Daylight and retail sales. California Energy Commission, 2003.

7 Hechong Mahone Group (HMG). Skylighting and retail sales. Pacific Gas and Electric, 1999.

8 CANMET. FRAMEplus 5.1: www.frameplus.net. Natural resources Canada, 2004.

9 LBNL. WINDOWS 5.1: http://windows.lbl.gov/. Lawrence Berkeley National Laboratory, March 2004.

10 LBNL, RADIANCE 3.5: http://radsite.lbl.gov/radiance/. Lawrence Berkeley National Laboratory, March 2004.

11 Lighting Technologies. LUMEN MICRO 2000: www.lighting-technologies.com. Lighting Technologies, Inc., March 2004.

12 IEA SHC Task 21. ADELINE 3.0, RADIANCE and SUPERLITE User's Manual. International Energy Agency, 2000.

13 HMG. SkyCalc: Skylighting tool for California and the Pacific Northwest. www.h-m-g.com. Hechong Mahone Group, March 2004.

14 Laouadi A., and Atif M.R. Transparent domed skylights: optical model for predicting transmittance, absorptance and reflectance. Lighting Research and Technology, 1998; 30(3): 111-118.

15 Laouadi A., and Atif M.R. Prediction models of optical characteristics for domed skylights under standard and real sky conditions: Proceedings of the 7th IBPSA conference, Rio de Janeiro, Brazil, 2001; 1101-1108.

16 Duffie J. A. and Beckman W. A. Solar Engineering of Thermal Processes. New York: John Wiley&Sons, Inc., 1991.

17 Perez R., Ineichen P., Seals R., Michalsky J., and Stewart R. Modeling daylight availability and irradiance components from direct and global irradiance. Solar Energy, 1990; 44(5): 271-289.

18 Wilkinson M. A., Natural lighting under translucent domes, Lighting Research Technology, 1992; 24(3): 117-126.

19 Muneer T., and Angus R.C. Daylight illluminance models for the United Kingdom. Lighting Research Technology, 1993; 25(3): 113-123.

20 ASTM Standard E972-96. Standard test method for solar photometric transmittance of sheet materials using sunlight. American Society for Testing and Materials, 1996.

21 ASTM Standard E1084-86/96. Standard test method for solar transmittance (terrestrial) of sheet materials using sunlight. American Society for Testing and Materials, 1996.

22 LBNL, Optics 5.1, Lawrence Berkeley National Laboratory: http://windows.lbl.gov/, March 2004.

23 Laouadi A. and Arsenault C. Validation of SkyVision. Report No. IRC-RR-167, http://irc.nrc-cnrc.gc.ca/ie/light/skyvision/publications.html. National Research Council of Canada: Ottawa, June 2004

24 Perez R., Seals R., and Michalsky J. All-weather model for sky luminance distribution – preliminary configuration and validation. Solar Energy, 1993; 50(3): 235-245.

25 CIE, Spatial distribution of daylight - luminance distributions of various reference skies. Report of the Commision Internationale de L'Eclairage, 1995.

26 IESNA. Lighting Handbook, Reference And Application Volume. New York: Illuminating Engineering Society of North America, 2000.

8 Appendix: Calculation of Coefficients γ_1, γ_2 and γ_3

8.1 Side Surface A_1 (or A_2)

Figure 13 shows a method to estimate the coefficient γ_1(or γ_2) for the diffuse sky light. Assuming a uniform sky luminance, the directly-transmitted portion of the incident flux on a given point on the surface A_1 (or A_2) of the vault skylight is proportional to the angle B. The coefficient γ_1 is then given by the following equation:

$$\gamma_1 = \gamma_2 = \frac{2B}{\pi F_{1b}} \tag{121}$$

with:

$$B = \cot an^{-1}(Z/L) = \cot an^{-1}\{R/L \cdot (\sin\sigma - \sin\sigma_0)\} \tag{122}$$

Equation (122) can be simplified to the following equation:

$$B = d_0 - d_1\{R/L \cdot (\sin\sigma - \sin\sigma_0)\} + d_2\{R/L \cdot (\sin\sigma - \sin\sigma_0)\}^2 \tag{123}$$

with:

$$\begin{aligned} &d_0 = \pi/2; \quad d_1 = 1.015; \quad d_2 = 0.233; \quad \text{for} \quad 0 \le R/L \le 2 \\ &d_0 = 0.803; \quad d_1 = 0.21; \quad d_2 = 0.0174; \quad \text{for} \quad 2 < R/L \le 6 \\ &d_0 = 0.213; \quad d_1 = 0.0106; \quad d_2 = 0.; \quad \text{for} \quad 6 < R/L \le 12 \end{aligned} \tag{124}$$

The average value of γ_1 over the surface A_1 becomes:

$$\bar{\gamma}_1 = \frac{4R^2}{\pi A_1 F_{1b}} \int_{\sigma_0}^{\pi/2} \left\{c_0 - c_1\{R/L(\sin\sigma - \sin\sigma_0)\} + c_2\{R/L(\sin\sigma - \sin\sigma_0)\}^2\right\} \cos^2\sigma \cdot d\sigma \tag{125}$$

Performing the integration in equation (125), one obtains:

$$\bar{\gamma}_1 = \frac{4}{\pi F_{1b}} \left\{ \begin{array}{l} 0.5 \cdot \left[d_0 + d_1 \cdot R/L \cdot \sin\sigma_0 + d_2 \cdot (R/L)^2 \left(1/4 + \sin^2\sigma_0\right)\right] - \\ \dfrac{R/L/3 \cdot \cos^3\sigma_0 \left(d_1 + d_2 \cdot (R/L) \cdot 5/4 \cdot \sin\sigma_0\right)}{\pi/2 - \sigma_0 - \sin\sigma_0 \cos\sigma_0} \end{array} \right\} \tag{126}$$

8.2 Top Surface A_3- Light Source Perpendicular to the Skylight Axis

Figure 14 shows a method to estimate the coefficient γ_3 for the diffuse sky light when the light source's rays are perpendicular to the skylight axis. Assuming a uniform sky luminance, the directly transmitted

portion of the incident flux on a given point on the surface A_3 of the vault skylight is proportional to the angle B. The coefficient γ_3 is then given by the following equation:

$$\gamma_{3,per} = \frac{B / F_{3b}}{A + B + C} = \frac{1 + 2\sigma_0 / \pi}{1 + 2\sigma / \pi} / F_{3b} \tag{127}$$

The average value of $\gamma_{3,per}$ over the surface A_3 becomes:

$$\bar{\gamma}_{3,per} = \frac{1}{S_3} \int_{A_3} \gamma_{3,per} \cdot ds = \frac{1 + 2\sigma_0 / \pi}{F_{3b}(1 - 2\sigma_0 / \pi)} \int_{\sigma_0}^{\pi/2} \frac{2 \cdot d\sigma / \pi}{1 + 2\sigma / \pi} \cdot d\sigma \tag{128}$$

Performing the integration in equation (128), one obtains:

$$\bar{\gamma}_{3,per} = \frac{1 + 2\sigma_0 / \pi}{F_{3b}(1 - 2\sigma_0 / \pi)} \cdot \ln\left(\frac{2}{1 + 2\sigma_0 / \pi}\right) \tag{129}$$

where the symbol (ln) stands for the logarithm of the base e.

8.3 Top Surface A_3- Light Source Parallel to the Skylight Axis

Figure 15 shows a method to estimate the coefficient γ_3 for the diffuse sky light when the light source's rays are parallel to the skylight axis. Assuming a uniform sky luminance, the directly transmitted portion of the incident flux on a given point on the surface A_3 of the vault skylight is proportional to the angle B. The coefficient γ_3 is then given by the following equation:

$$\gamma_{3,par} = \frac{B / F_{3b}}{\pi} \tag{130}$$

with:

$$B = \tan^{-1}\left(\frac{Y/R}{1 - \sin\sigma_0}\right) + \tan^{-1}\left(\frac{L/R - Y/R}{1 - \sin\sigma_0}\right) \tag{131}$$

The average value of $\gamma_{3,par}$ over the surface A_3 becomes:

$$\bar{\gamma}_{3,par} = \frac{1}{S_3} \int_{A_3} \gamma_{3,par} \cdot ds = \frac{R/L}{\pi F_{3b}} \int_0^L \left\{ \tan^{-1}\left(\frac{Y/R}{1 - \sin\sigma_0}\right) + \tan^{-1}\left(\frac{L/R - Y/R}{1 - \sin\sigma_0}\right) \right\} dY/R \tag{132}$$

Performing the integration in equation (132), one obtains:

$$\bar{\gamma}_{3,par} = \frac{2}{\pi F_{3b}} \left\{ \tan^{-1}\left(\frac{L/R}{1 - \sin\sigma_0}\right) - \frac{1}{2} R/L(1 - \sin\sigma_0) \cdot \ln\left(1 + \left(\frac{L/R}{1 - \sin\sigma_0}\right)^2\right) \right\} \tag{133}$$

Since the sky luminance is assumed uniform, the average value of γ_3 over the surface A_3 for both the perpendicular and parallel configurations reads as follows:

$$\gamma_3 = \left(\gamma_{3,per} + \gamma_{3,par}\right)/2 \tag{134}$$

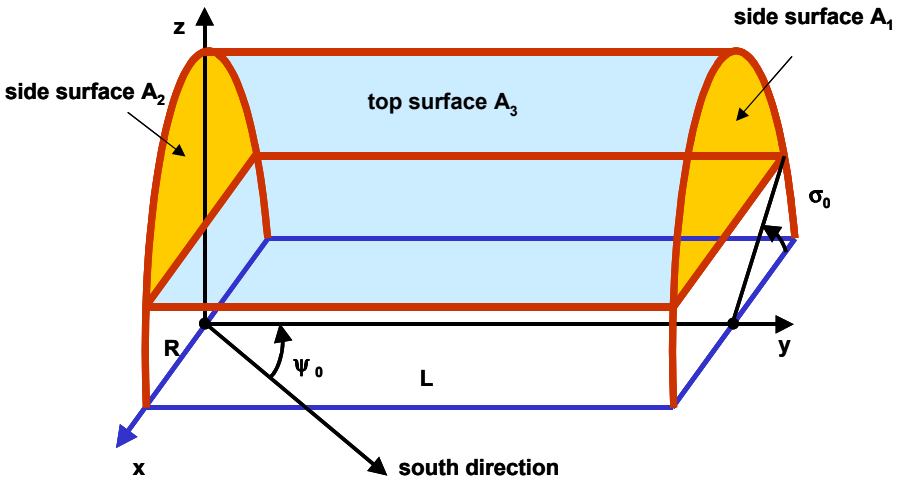

Figure 1 Schematic description of a barrel vault skylight

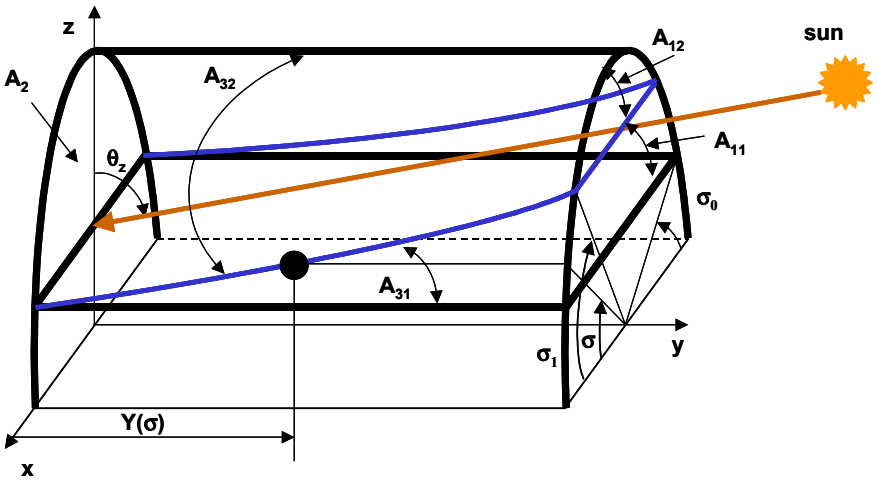

Figure 2 Beam light transmission –sun's rays parallel to the skylight axis

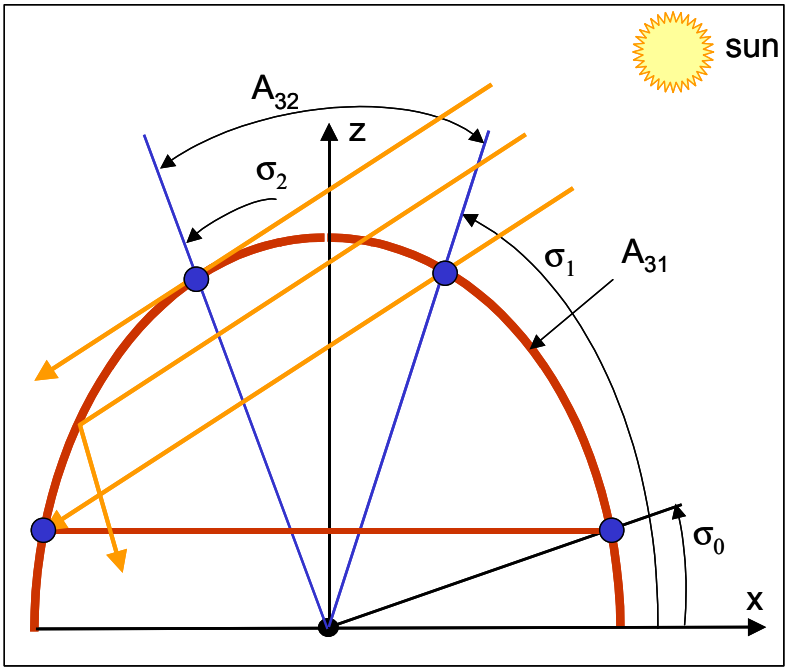

Figure 3 Beam light transmission–sun's rays perpendicular to the skylight axis

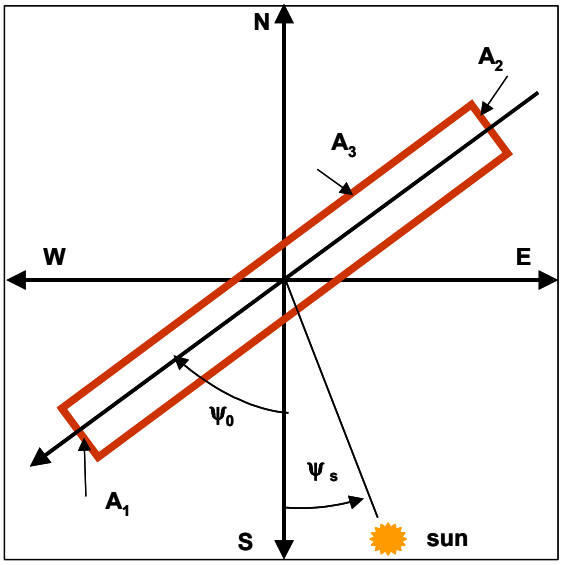

Figure 4 Position of the skylight with respect to the sun and the four cardinal directions

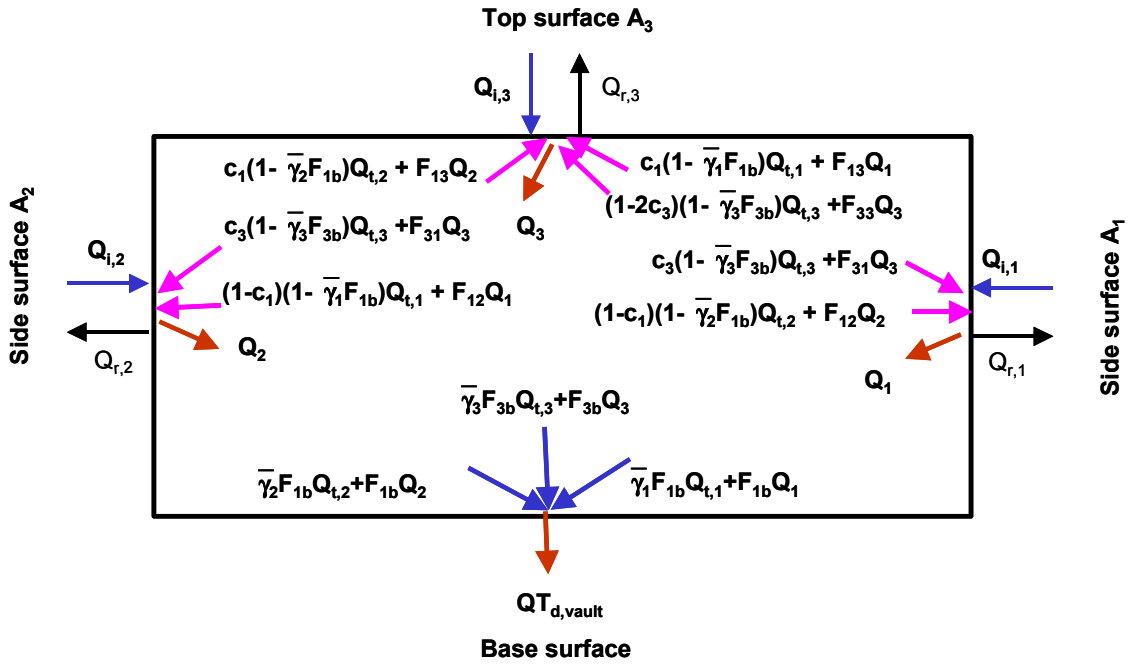

Figure 5 Diffuse light transmission through a barrel vault skylight

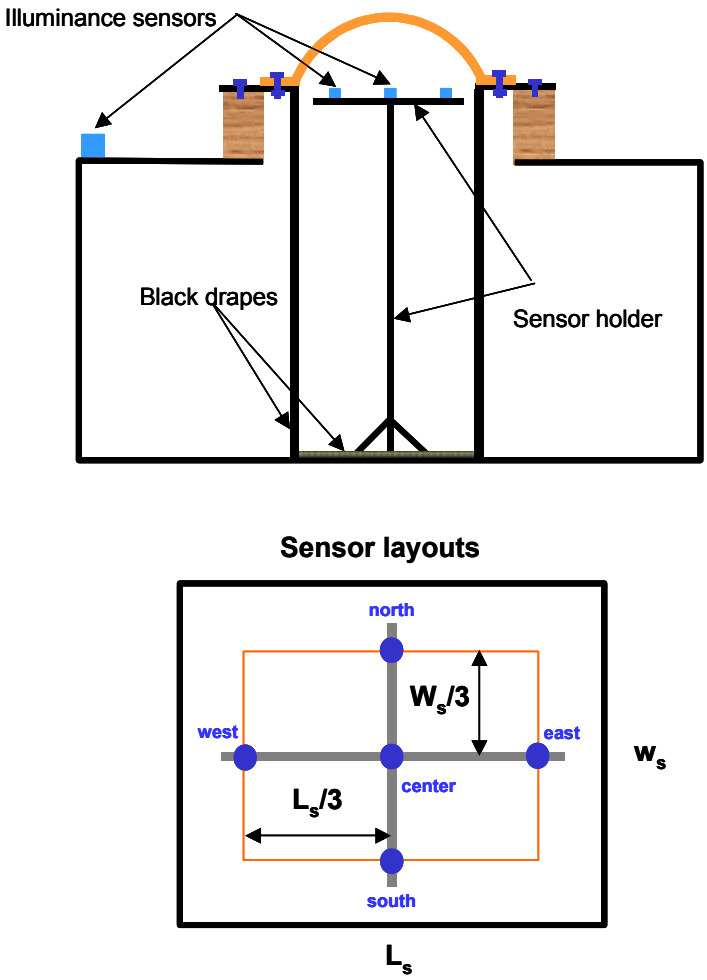

Figure 6 Schematic description of the skylight equivalent visible transmittance measurement setup and sensor layouts

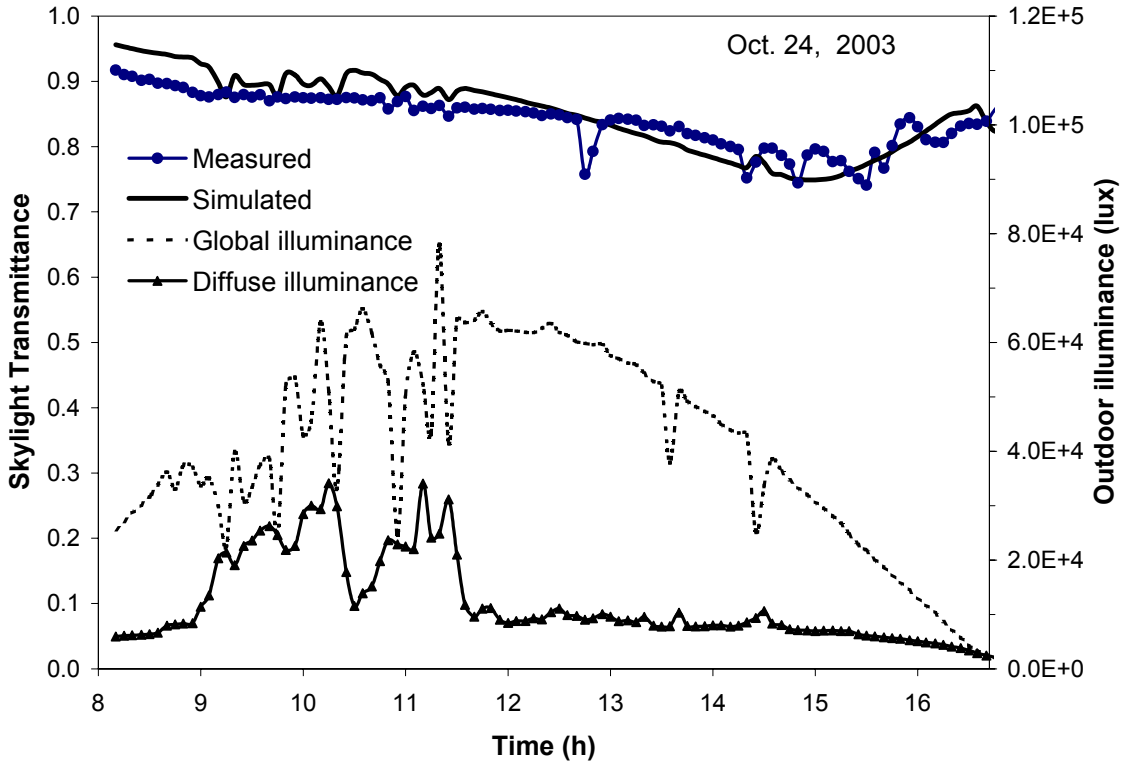

Figure 7 Skylight equivalent visible transmittance for the combined sun beam and sky diffuse light - comparison between the actual measurements and model predictions

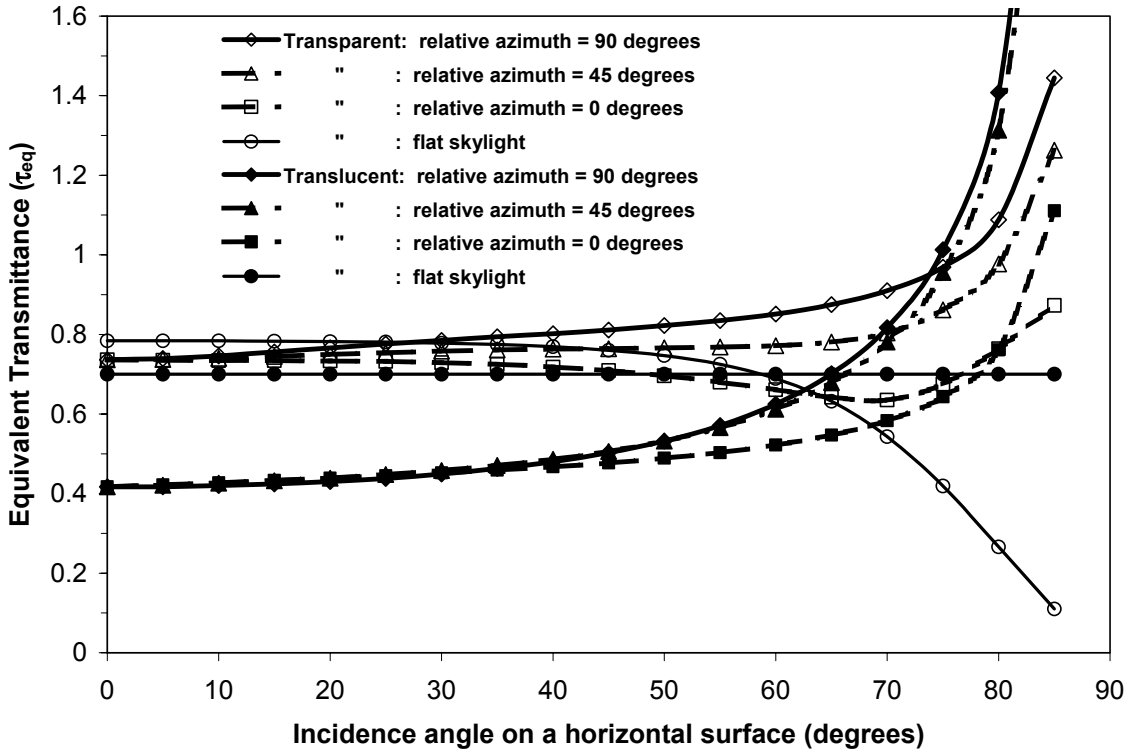

Figure 8 Profiles of the beam equivalent transmittance of fully transparent and translucent vault skylights as a function of the incidence angle on a horizontal surface

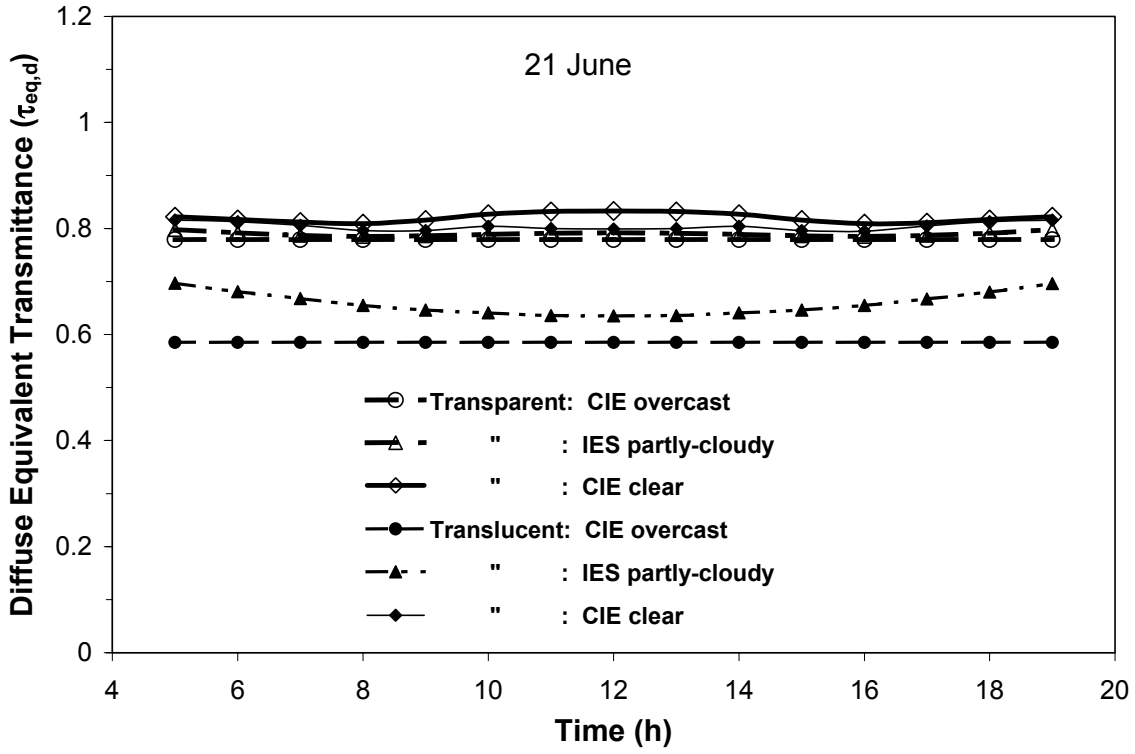

Figure 9 Daily profiles of the diffuse equivalent transmittance of fully transparent and translucent vault skylights under standard sky conditions during typical summer day

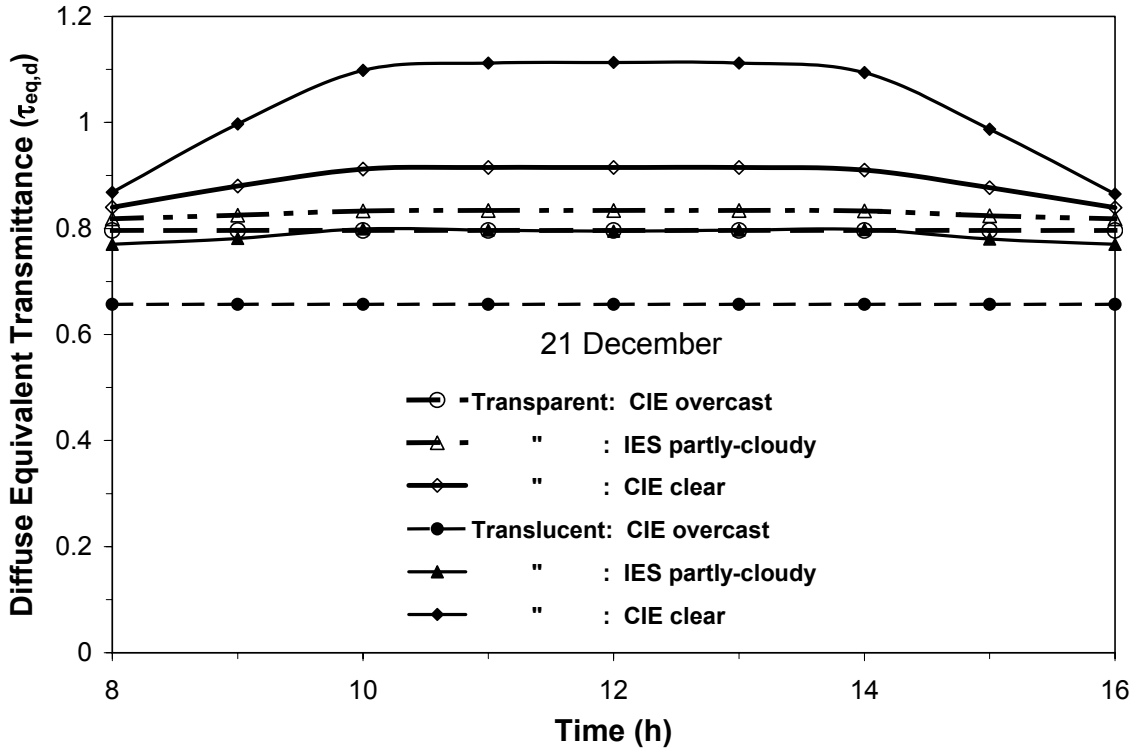

Figure 10 Daily profiles of the diffuse equivalent transmittance of fully transparent and translucent vault skylights under standard sky conditions during typical winter day

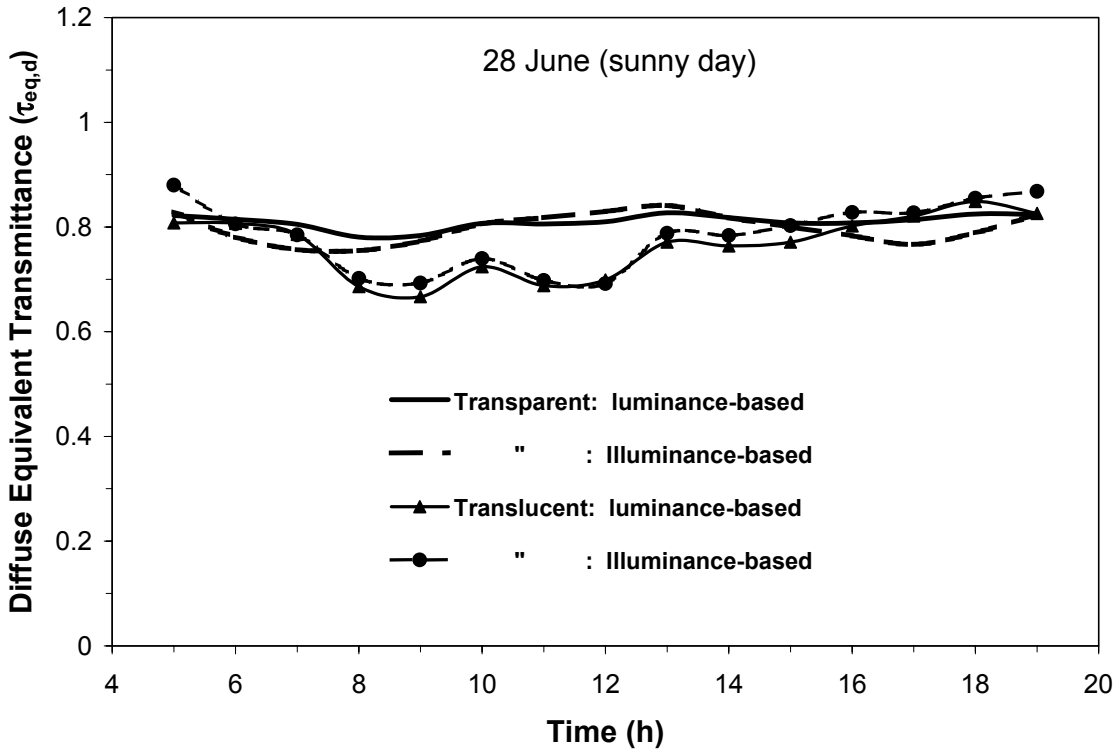

Figure 11 Comparison between the predictions from the luminance-based and illuminance-based models under dynamic sky conditions of typical summer sunny day

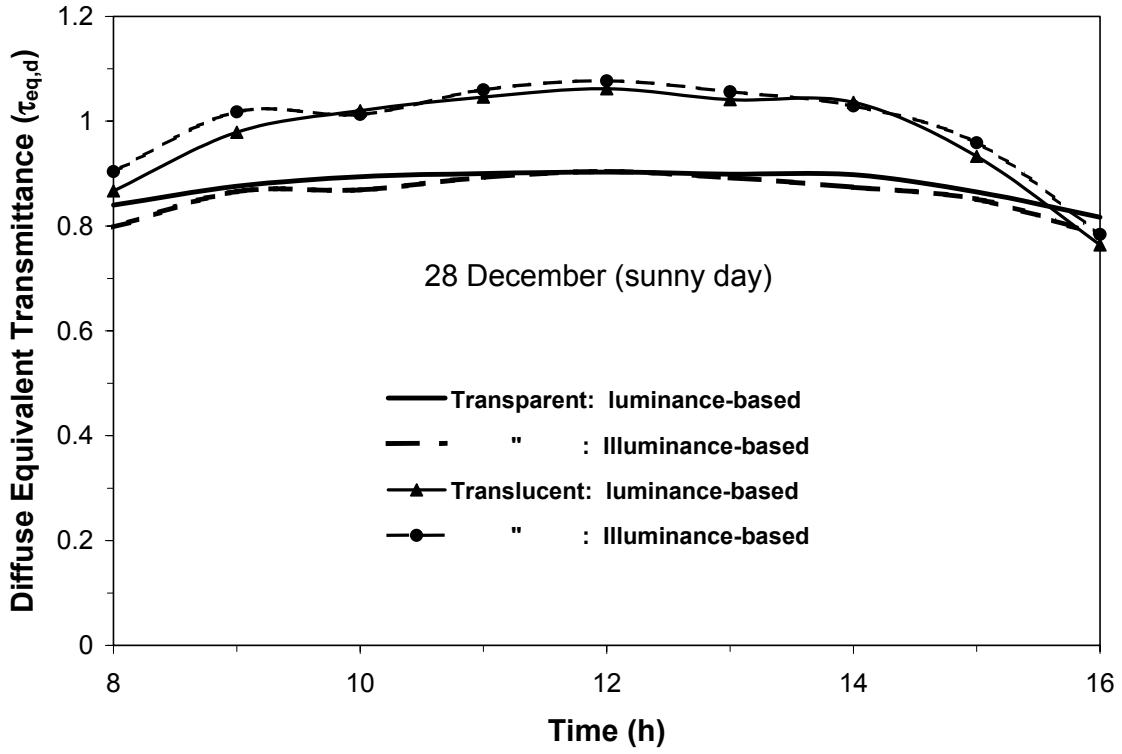

Figure 12 Comparison between the predictions from the luminance-based and illuminance-based models under dynamic sky conditions of typical winter sunny day

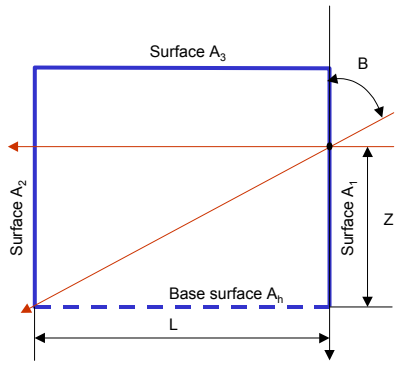

Figure 13 Calculation of the coefficient γ_1

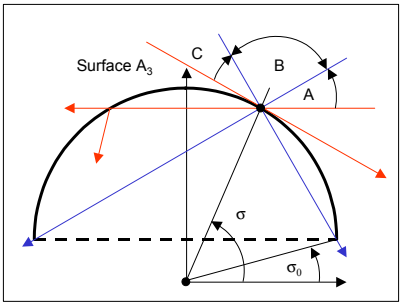

Figure 14 Calculation of the coefficient γ_3–source's rays perpendicular to the skylight axis

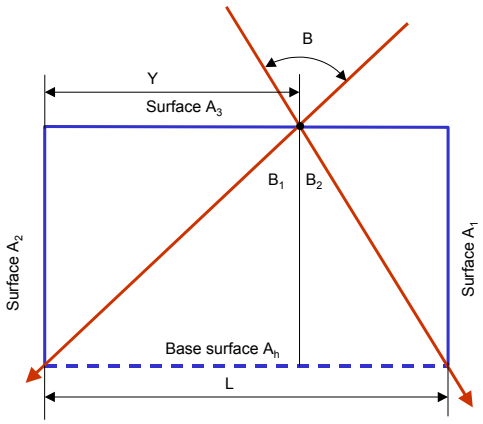

Figure 15 Calculation of the coefficient γ_3–source's rays parallel to the skylight axis